

[FeFe]-Hydrogenase H-Cluster Mimics with Various $-\text{S}(\text{CH}_2)_n\text{S}-$ Linker Lengths ($n = 2-8$): A Systematic Study

Hassan Abul-Futouh,[†] Laith R. Almazahreh,^{†,‡} Mohammad Kamal Harb,[§] Helmar Görls,[†] Mohammad El-khateeb,^{||} and Wolfgang Weigand^{*,†}

[†]Institut für Anorganische und Analytische Chemie, Friedrich-Schiller-Universität Jena, Humboldt Str. 8, 07743 Jena, Germany

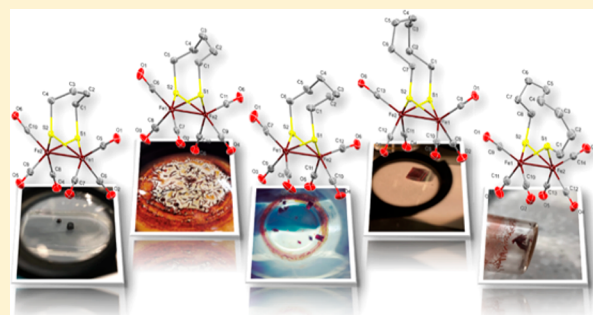
[‡]ERCOSPLAN Ingenieurbüro Anlagentechnik GmbH, Arnstädter Straße 28, 99096 Erfurt, Germany

[§]Department of Pharmacy, Al-Zytoonah University of Jordan, P.O. Box 130, Amman 11733, Jordan

^{||}Chemistry Department, Jordan University of Science and Technology, Irbid 22110, Jordan

Supporting Information

ABSTRACT: The effect of the nature of the dithiolato ligand on the physical and electrochemical properties of synthetic H-cluster mimics of the [FeFe]-hydrogenase is still of significant concern. In this report we describe the cyclization of various alkanedithiols to afford cyclic disulfide, tetrasulfide, and hexasulfide compounds. The latter compounds were used as proligands for the synthesis of a series of [FeFe]-hydrogenase H-cluster mimics having the general formulas $[\text{Fe}_2(\text{CO})_6\{\mu\text{-S}(\text{CH}_2)_n\text{S}\}]$ ($n = 4-8$), $[\text{Fe}_2(\text{CO})_6\{\mu\text{-S}(\text{CH}_2)_n\text{S}\}_2]$ ($n = 6-8$), and $[\text{Fe}_2(\text{CO})_6\{\mu\text{-S}(\text{CH}_2)_n\text{S}\}_2]$ ($n = 6-8$). The resulting complexes were characterized by ^1H and $^{13}\text{C}\{^1\text{H}\}$ NMR and IR spectroscopic techniques, mass spectrometry, and elemental analysis as well as X-ray analysis. The purpose of this research was to study the influence of the systematic increase of n from 2 to 7 on the redox potentials of the models and the catalytic ability in the presence of acetic acid (AcOH) by applying cyclic voltammetry.



INTRODUCTION

In step with population growth, the increased consumption of fossil fuels has led to the greenhouse effect and global warming.¹ Therefore, finding alternative energy sources is essential to meet the inexorable rise of the energy demand. Hydrogen is a zero-emission fuel when burned, and it is characterized by high energy density.^{2a} In addition, hydrogen is essential for the fertilizer economy (e.g., nitrate of potash (NOP) production), where ammonia is produced via the Haber–Bosch process.^{2b,c} The cleanest way to produce hydrogen is via water electrolysis using platinum catalysts,³ which limits the wide spread of the hydrogen economy. Accordingly, the challenge is to develop a cheap, efficient, and robust electrocatalyst as an alternative to platinum. In biological processes, hydrogen production or consumption are catalyzed by enzymes known as [FeFe]-hydrogenases.⁴⁻⁶ The active site of these enzymes contains an organometallic Fe/S cluster, the so-called H-cluster (Figure 1a), that is responsible for the catalytic process.⁷

Over the past few decades, several diiron dithiolato complexes that mimic the butterfly $[\text{Fe}_2\text{S}_2]$ subcluster of the H-cluster have been synthesized by altering the bridge in $[\text{Fe}_2(\text{CO})_6\{\mu\text{-S}(\text{bridge})\text{S}\}]$ (Figure 1b) and tested as electrocatalysts.⁸⁻¹⁶ Moreover, these complexes have been modified to contain heavier chalcogen atoms such as selenium or tellurium instead of sulfur.¹⁷ In addition, substitution of the CO ligands

in $[\text{Fe}_2(\text{CO})_6\{\mu\text{-S}(\text{CH}_2\text{YCH}_2)\text{S}\}]$ ($\text{Y} = \text{CH}_2, \text{NR}, \text{O}, \text{SiR}_2, \text{PhP}=\text{O}$) by cyanide,¹⁸ phosphanes,^{12f,13a,19} phosphites,^{12f,13a,19b-1} carbenes,^{12m,13d,19b,20} nitrosyl,²¹ or sulfides^{18b,22} to produce mono-, di-, tri-, and tetrasubstituted complexes has been extensively studied.^{12m,18-22} Furthermore, other efforts have focused on synthesizing macrocyclic complexes that contain two $[\text{Fe}_2\text{S}_2]$ clusters connected by different linkers, which provide two catalytic active centers. The first example of such macrocycles that have nonsymmetric linkers was reported by Song and co-workers in 2002.^{23a} Later, Song also described the synthesis of a complex containing two $[\text{Fe}_2\text{S}_2]$ clusters connected by two equivalent butyl chains, forming a 16-membered macrocycle.^{23d} However, such unique architectures are rare, and only few examples are known.^{15a,23} It is worth pointing out that diiron complexes with the general formula $[\text{Fe}_2(\text{CO})_6\{\mu\text{-}(\text{SR})_2\}]$ may adopt three possible stereoisomers based on the orientation of the R substituents: axial–axial (*aa*), axial–equatorial (*ae*), and equatorial–equatorial (*ee*), as illustrated in Figure 1c.⁸ Whereas chelating dithiolato organic substituents, such as 1,2-ethanedithiolate (edt) and 1,2-propanedithiolate (pdt), always form the *aa* isomer, non-chelating ones like methyl (Me) and ethyl (Et) groups give

Received: June 1, 2017

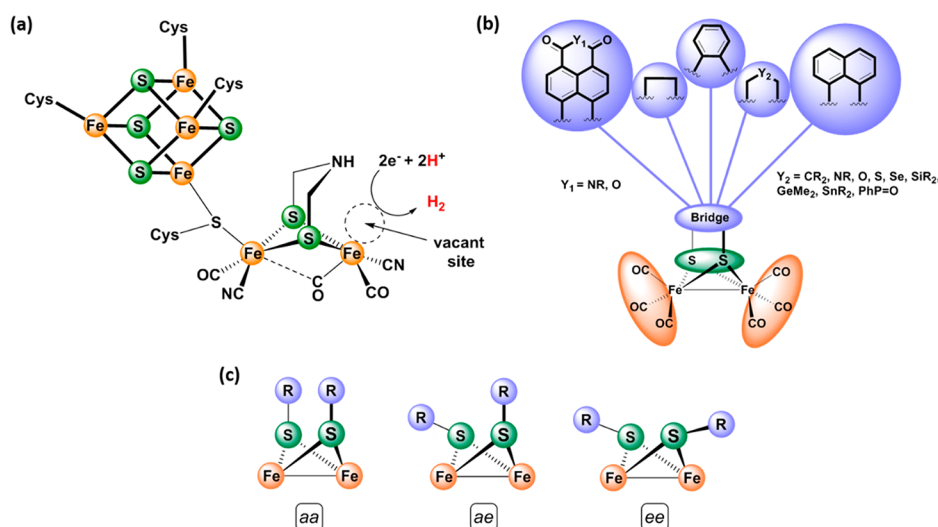


Figure 1. (a) Structure of the H-cluster. (b) Synthetic models of the active site of [FeFe]-hydrogenase. (c) Three isomers of diiron dithiolato carbonyls (CO ligands have been omitted for clarity).

only a mixture of the *ae* and *ee* isomers in different ratios based on the nature of the R substituents.⁸

In the total picture, a basic aim of the synthetic chemistry is to mimic the electronic and structural characteristics of the [Fe₂S₂] core of the H-cluster and to provide a good understanding of the factors stabilizing its rotated state. In fact, within the numerous complexes for the reduced state of the H-cluster (H_{red}), in which the two iron units are in a fully or distorted eclipsed conformation, only two [Fe^IFe^I] complexes featuring the rotated structure have been reported,^{24a,b} and one complex exhibits a semirotated state.^{24c} Remarkably, the steric bulk of the dithiolato linker and asymmetrical coordination at the two Fe atoms play a crucial role in stabilizing the rotated/semirotated states of these complexes. On the other hand, the reduction of [Fe^IFe^I] hexacarbonyl complexes, e.g., [Fe₂(CO)₆{μ-S(C₆H₄)S}],^{11b} may trigger inversion of one of the Fe(CO)₃ units to locate one CO ligand in a semibridging position for stabilization of the negative charge.^{9b,11a,c–e,g,17e,25}

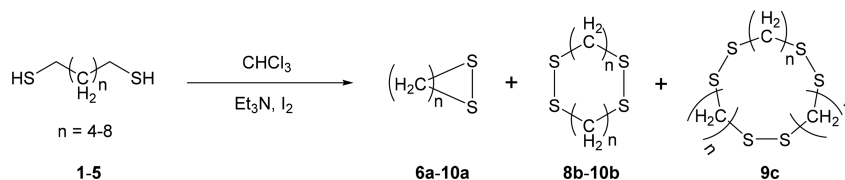
One focus of our group is to investigate the effect of the nature of the dithiolato ligand on the physical and electrochemical properties of the diiron dithiolato complexes. In this respect, we have published several studies in which we systematically altered the structure of the ligand [–XCH₂YCH₂X–] as follows: (1) X = S is replaced by X = Se or Te, which results in an increase in the electron-richness at the diiron core in going from S to Se to Te, accompanied by a decrease in the reduction potential of the model system.^{17c} (2) The presence of Y = S or Se instead of O leads to an ECE reduction mechanism (E = electron transfer, C = chemical process) due to a facile core reorganization accompanying the electron transfer.^{17a} (3) Increasing the steric bulkiness of Y (CH₂, CHMe, CMe₂) lowers the barrier for Fe(CO)₃ rotation and results in an ECE reduction mechanism only in the case of Y = CMe₂.^{17c} (4) The introduction of heavier group 14 atoms at the bridgehead position (Y) stabilizes the –SCYCS– moiety in a nearly planar state for Y = GeMe₂ or SnMe₂.^{15a} We have also confirmed that the electron density of the μ-S atoms (and hence that of Fe–Fe bond)^{15a} increase in going from CMe₂ to SiMe₂ to GeMe₂ to SnMe₂ and that protonation of the Fe–Fe bond using the moderately strong acid CF₃CO₂H can be accomplished in the case of Y = SnMe₂ and X = Se.^{17d}

Herein we report the cyclization of different alkanedithiols by means of the high-dilution technique to afford cyclic disulfides, tetrasulfides, and hexasulfides (**6a–10a**, **8b–10b**, and **9c**, respectively; Table 1). The resulting compounds were fully characterized by a variety of analytical techniques (NMR spectroscopy, elemental analysis, mass spectrometry, and X-ray structure determination of compounds **8b–10b** and **9c**). Subsequently, these compounds were used as proligands to synthesize a series of complexes of the type [Fe₂(CO)₆{μ-S(CH₂)_nS}] (*n* = 4–8) (**13–17**), [Fe₂(CO)₆{μ-S(CH₂)_nS}]₂ (*n* = 6–8) (**18–20**), and [Fe₂(CO)₆{(μ-S(CH₂)_nS)₂}] (*n* = 6–8) (**21–23**). The molecular structures of complexes **13–20** and **22** were determined using single-crystal X-ray diffraction analysis. In addition, we also resynthesized the known complexes [Fe₂(CO)₆{μ-S(CH₂)₂S}] (**11**)^{26a} and [Fe₂(CO)₆{μ-S(CH₂)₃S}] (**12**)^{26b} to study how the physical, electrochemical, and electrocatalytic features are influenced by the systematic increase of *n* from 2 to 8 in complexes **11–17**.

RESULTS AND DISCUSSION

Synthesis and Characterization of Cyclic Di-, Tetra-, and Hexasulfides. The synthetic procedures and characterizations of the precursors **1–5** required for the preparation of compounds **6a–10a**, **8b–10b**, and **9c** are described in detail in the Supporting Information. The syntheses of the cyclic disulfides (**6a–10a**), tetrasulfides (**8b–10b**), and hexasulfide (**9c**) were carried out by following the high-dilution technique previously described in the literature (Table 1).²⁷ Simultaneous addition of solutions of the dithiols and excess I₂ in CHCl₃ to a vigorously stirred solution of Et₃N in CHCl₃ followed by column chromatography afforded the disulfides with *n* = 4 and 5 (**6a** and **7a**), while for *n* = 6–9 the same mixture had two products, the disulfides (**8a–10a**) and the tetrasulfides (**8b–10b**) (Table 1). In the case of *n* = 7, trace amounts of the hexasulfide (**9c**) were obtained. To the best of our knowledge, compounds **9b** and **9c** are reported for the first time in this paper, and the yields of compounds **6a–10a**, **8b**, and **10b** obtained by this method are higher than those reported in the literature.²⁸ Single crystals of compounds **8b–10b** and **9c** were obtained from saturated solutions of hexane at –20 °C for X-ray diffraction studies. The molecular structures of these

Table 1. Synthetic Pathway for Compounds 6a–10a, 8b–10b, and 9c



Entry	Product					
	Cyclic disulfide	Isolated yield (%)	Dimeric disulfide	Isolated yield (%)	Trimeric disulfide	Isolated yield (%)
HS(CH ₂) ₄ SH (1)	 6a	95%	-	-	-	-
HS(CH ₂) ₅ SH (2)	 7a	90%	-	-	-	-
HS(CH ₂) ₆ SH (3)	 8a	65%	 8b	25%	-	-
HS(CH ₂) ₇ SH (4)	 9a	65%	 9b	15%	 9c	15%
HS(CH ₂) ₈ SH (5)	 10a	75%	 10b	20%	-	-

compounds (Figure 2) show cyclic molecules consisting of methylene chains in a zigzag conformation linked by disulfide bonds. The average C–C–C bond angles of **8b–10b** and **9c** are around 113.4° indicating an sp³ hybridized C atoms, while the average C–C bond distance of these compounds is ~1.524 Å, a typical value for cyclic hydrocarbons.^{29a,b} In addition, the average S–S bond distance is 2.0394 Å which is in agreement with the corresponding bond in α-S₈ (2.05 Å)^{29c} and the average dihedral angles between the planes through the two sets of C–S–S and S–S–C atoms are 82.02° for the compounds **8b–10b** and **9c**.

Synthesis and Characterization of Dinuclear and Tetranuclear Complexes 13–23. The dinuclear complexes **13–17** were synthesized as shown in Scheme 1. Unexpectedly, neither the reaction of in situ-generated (μ-LiS)₂Fe₂(CO)₆ with 1 equiv of alkyl dibromide [Br(CH₂)_nBr] (*n* = 4–8) (Scheme 1A) nor the reaction of alkyldithiol [SH(CH₂)_nSH] (*n* = 4–8) with Fe₃(CO)₁₂ in boiling THF (Scheme 1B) afforded the

dinuclear complexes **13**³¹–**17**. In contrast, the reactions of compounds **6a–10a** with equimolar amounts of Fe₃(CO)₁₂ in boiling THF for 1 h followed by column chromatography afforded the dinuclear complexes **13–17**, as illustrated in Scheme 1C. Complexes **13–17** could be formed by the general route proposed by Nametkin and co-workers,³⁰ in which thermal decomposition of Fe₃(CO)₁₂ takes place initially to afford the unsaturated 16-electron species Fe(CO)₄, which subsequently reacts with the disulfide sulfur atoms to generate [(OC)₄FeSRSFe(CO)₄] as an intermediate. The latter then releases two CO ligands to afford complexes **13–17**.

Otherwise, the reaction of 2 equiv of Fe₃(CO)₁₂ with 1 equiv of **8b–10b** in boiling THF for 2 h afforded the tetranuclear complexes **18–20**, whereas the reaction of Fe₃(CO)₁₂ with compounds **8b–10b** in a 1:1 molar ratio under the same conditions with the same separation procedure afforded complexes **21–23** containing one [Fe₂S₂] subcluster as well as traces of the tetranuclear complexes **18–20** (Scheme 2). The

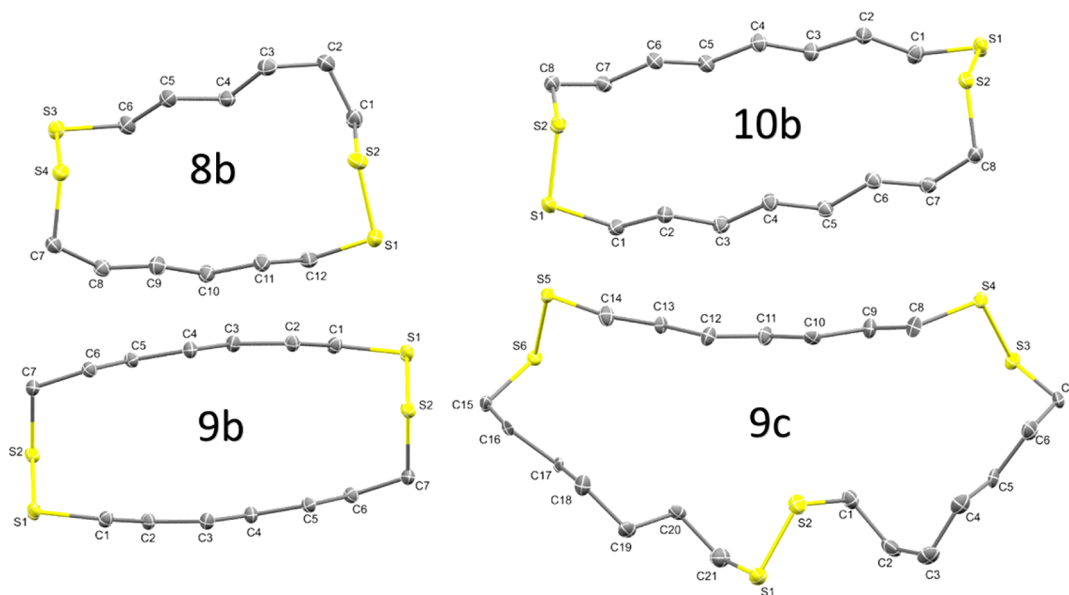
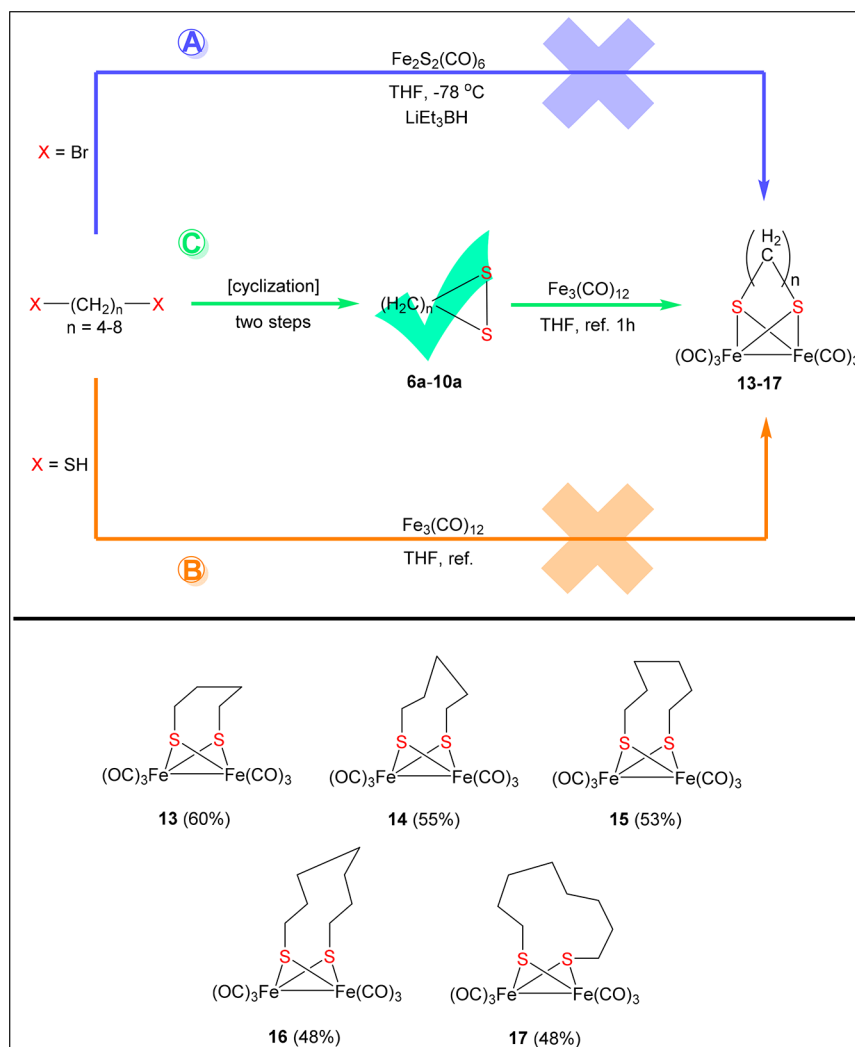


Figure 2. Molecular structures (50% probability) of compounds **8b–10b** and **9c**. Hydrogen atoms have been omitted for clarity.

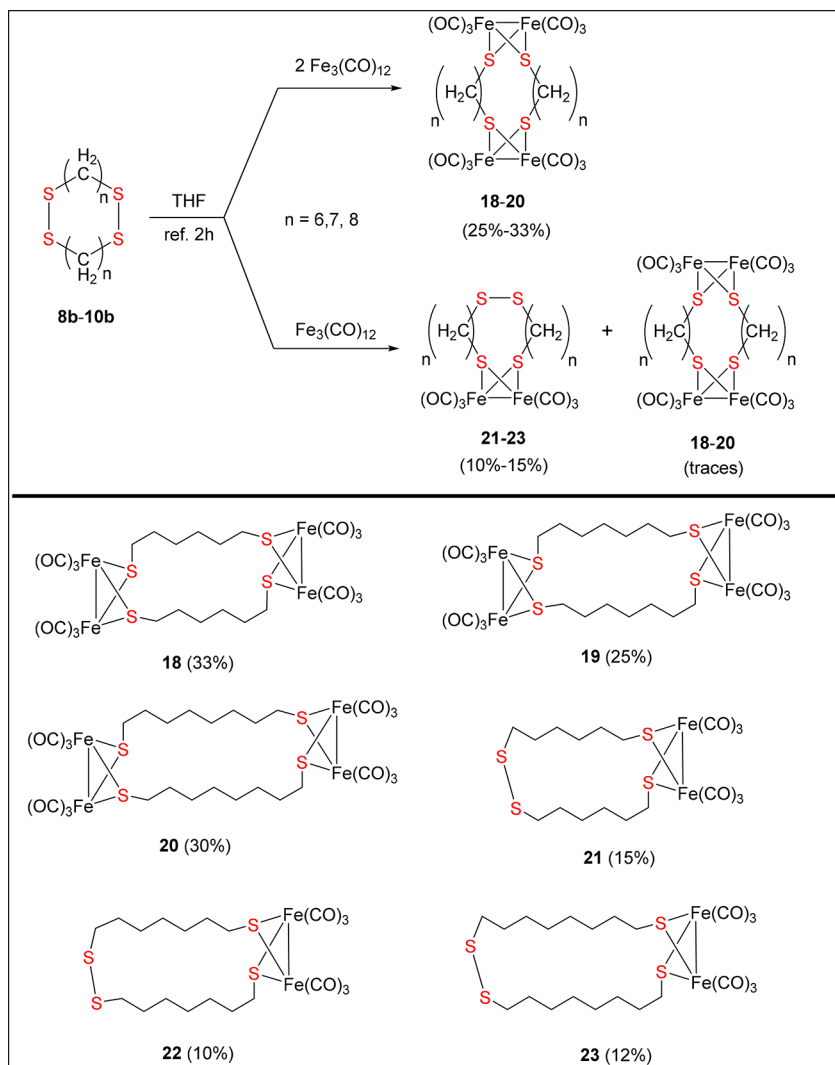
Scheme 1. Attempts To Prepare the Dinuclear Complexes **13–17**



resulting complexes **13–23** were characterized by spectroscopic techniques (^1H NMR, $^{13}\text{C}\{^1\text{H}\}$ NMR (except for complexes

21–23), and IR), mass spectrometry, and elemental analysis as well as X-ray crystallography for complexes **13–20** and **22**.

Scheme 2. Synthetic Pathways for Complexes 18–23



The IR spectra of complexes **13–17** and those of complexes **18–23** in CH_2Cl_2 are nearly identical to each other in terms of the number of peaks and frequencies (Table S1 in the Supporting Information). It is evident from Table S1 that the average $\nu(\text{CO})$ wavenumbers shift to slightly smaller values in going from **11** to **17**, which indicates that increasing the length of the dithiolato bridge does not harshly change the electron-donating ability of the dithiolato bridge. The ^1H NMR spectra of the dinuclear complexes **13–16** show signals at 2.59, 2.61, 2.49, and 2.30 ppm for protons in the methylene groups attached directly to $\mu\text{-S}$ and another set of signals at 1.66, 1.75, 1.64, and 1.60 ppm for the SCH_2CH_2 moieties. Furthermore, the signals of the protons in the rest of the methylene groups of the chain linkers appear at 1.56 ppm for complex **14** and 1.53 ppm for complex **15**, while those of complex **16** appear at 1.48 and 1.38 ppm.

On the other hand, the ^1H – ^1H COSY analysis of **17** allowed the assignment of the ^1H NMR resonances of the two singlets with an equal intensity at 2.45 and 2.18 ppm to the protons in the SCH_2 moieties located at the equatorial (*e*) and axial (*a*) positions, respectively. Thus, the two signals at 1.87 and 1.54 ppm were assigned to the protons of the *e* and *a* CH_2 groups in SCH_2CH_2 moieties, while the three signals at 1.63, 1.44, and 1.34 ppm were assigned to the remaining protons in the chain

linker. The $^{13}\text{C}\{^1\text{H}\}$ NMR spectra display one signal for the carbonyl carbon atoms at 207.9 ppm for complex **13** and at 207.7 ppm for complexes **14–16**, whereas for complex **17** the signal appears at 209.4 ppm. The signals for the methylene carbons in the chain linkers were also detected in the range of 23.4–37.4 ppm for complexes **13–17** (see the Experimental Section). In the case of the tetranuclear complexes **18–20**, the ^1H NMR spectra exhibit two signals in the range of 2.08–2.47 ppm for the methylene protons connected to the $\mu\text{-S}$ atoms and located at the *e* and *a* positions. Another set of signals was detected in the range of 1.59–1.75 ppm for the protons in the SCH_2CH_2 moieties, as was a multiplet in the range of 1.26–1.52 ppm for protons in the remaining CH_2 groups. Similar to the dinuclear complexes, the $^{13}\text{C}\{^1\text{H}\}$ NMR spectra of complexes **18–20** showed one singlet for the carbonyl carbon atoms, at 208.9 ppm for complexes **18** and **19** and at 209.1 ppm for complex **20**. Besides, the signals of the methylene carbon atoms of the chain linker were detected in the range of 23.84–39.37 ppm (see the Experimental Section). Moreover, the ^1H NMR spectra of complexes **21–23** show broad signals at 2.71, 2.75, and 2.72 ppm, respectively, for the methylene protons connected to the S–S bond. Another two singlets with the same intensity for complexes **21** (2.51 and 2.14 ppm), **22** (2.50 and 2.11 ppm), and **23** (2.52 and 2.15 ppm) were assigned to

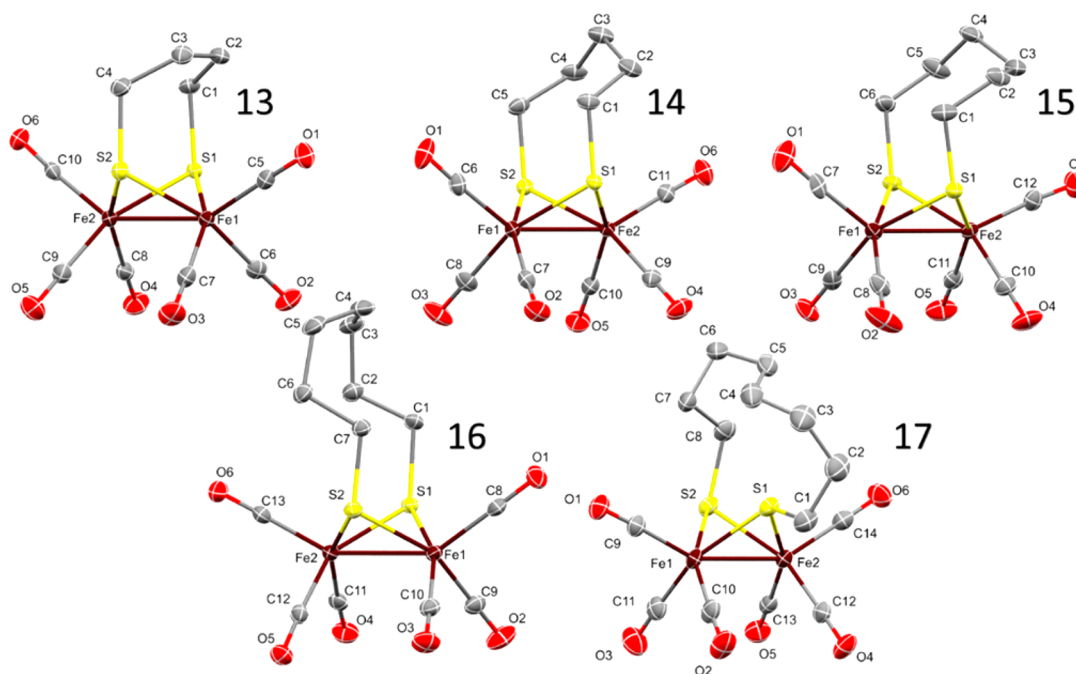


Figure 3. Molecular structures (50% probability) of complexes 13–17. Hydrogen atoms have been omitted for clarity.

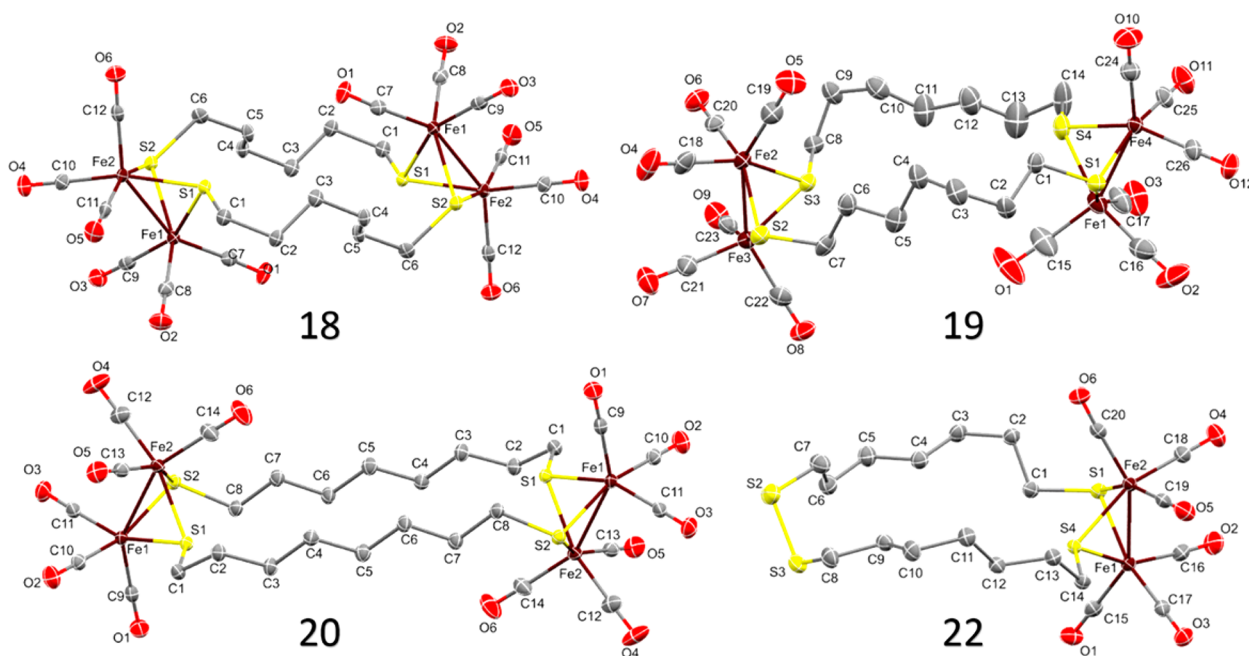


Figure 4. Molecular structures (50% probability) of complexes 18–20 and 22. Hydrogen atoms have been omitted for clarity.

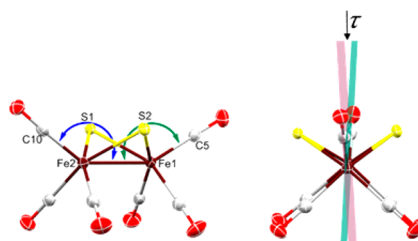
the methylene protons attached to the single $[\text{Fe}_2\text{S}_2]$ subcluster. This implies that these CH_2 moieties are oriented in the a and e positions. The mass spectra of complexes 13–23 showed the molecular ion peaks and the peaks resulting from dissociation of the CO ligands sequentially.

Molecular Structures. Single crystals suitable for X-ray diffraction studies were obtained from pentane-saturated solutions of complexes 13–17 at -20°C , while those for 18–20 and 22 were obtained by diffusion of hexane into CH_2Cl_2 solutions also at -20°C . The molecular structures of complexes 13–20 and 22 are shown in Figures 3 and 4, and selected bond lengths and angles for complexes 13–17 are given in Table 2. Three crystallographically independent

molecules in the unit cell of complex 15 were determined; only one of them is shown in Figure 3.

It is evident from Figure 3 that each complex has a butterfly $[\text{Fe}_2\text{S}_2]$ -cluster core that contains a bridging alkyldithiolato linker $[\mu\text{-S}(\text{CH}_2)_n\text{S}\text{-}\mu]$ ($n = 4\text{--}8$) and that each iron atom is bonded to three carbonyl ligands, similar to the corresponding complexes 11 and 12 reported in the literature.²⁶ The two S–C bonds are in axial positions with exception of complex 17, in which one S–C is axial and the other one is equatorial. Such orientation was also observed by Song and co-workers for $[\text{Fe}_2(\text{CO})_6\{\mu\text{-SCH}_2(\text{CH}_2\text{OCH}_2)_n\text{CH}_2\text{S}\text{-}\mu\}]$ ($n = 3, 4$).^{23b} The Fe–Fe bond lengths of complexes 13–17 are very close to those in the corresponding complexes 11 and 12 (Table 2), as

Table 2. Structural Comparison of Complexes 13–17



Complex	Fe2-Fe1 (Å)	S1...S2 (Å)	C10-Fe2-Fe1-C5, (τ) ^(°) ^b	Fe-Fe-C10, C5 (°)
11 ^{26a}	2.505(1)	2.892(2)	6.3(6)	149.7(2), 149.0(2)
12 ^{26b}	2.5105(9)	3.050	0.0(3)	148.32(9), 148.32(9)
13	2.5179(3)	3.0930(4)	6.6(1)	144.93(5), 151.25(5)
14	2.5178(3)	3.1403(5)	8.2(2)	152.82(6), 144.92(6)
15 ^a	2.5188(14)	3.1737(4)	6.83(7)	155.07(2), 144.84(3)
16	2.5074(2)	3.2135(4)	12.6(1)	151.79(4), 145.26(4)
17	2.4997(4)	2.8434(6)	2.0(2)	149.40(6), 154.48(6)

^aAverage of three independent molecules. ^bTorsion angle formed from the intersection between the apical carbonyl carbon atoms across the Fe–Fe bond.

is the average Fe–CO bond length (1.801 Å). Furthermore, the distance between the two sulfur atoms is slightly increased in going from 13 to 16 compared with complexes 11 and 12, while in the case of complex 17 it becomes shorter than those of 11 and 12 (see Table 2). In addition, it is clear from the torsion angle (τ), formed from the intersection between (O)C–Fe–Fe–C(O), together with the Fe–Fe–C(O) angles (Table 2) that the steric characteristics of the chain linkers distort the symmetry of the Fe(CO)₃ portion of the molecule. In the case of the tetranuclear complexes 18–20 and complex 22, Figure 4 confirms that complexes 18–20 are composed of two butterfly [Fe₂S₂]-cluster cores that are linked together by alkyl chains [–(CH₂)_n–] ($n = 6–8$) to form 20-, 22-, and 24-membered macrocyclic complexes, respectively. Complex 22 contains only one butterfly [Fe₂S₂]-cluster core bridged by the linker [–(CH₂)₇SS(CH₂)₇–] to form a 20-membered macrocyclic complex. All of the S–C bonds are in *e* and *a* positions, and their average bond lengths (*e*, 1.826 Å; *a*, 1.836 Å) are in agreement with those in the corresponding reported complexes.²³ Moreover, the average Fe–Fe bond length (2.513 Å) is in agreement with that in complex 12, which emphasizes that the formation of the macrocycle has no influence on the Fe–Fe distance.

Electrochemical Investigation. Table 3 summarizes the redox potentials of complexes 11–16 in CH₂Cl₂/[*n*-Bu₄N][BF₄] obtained by cyclic voltammetry. The cyclic voltammograms of the complexes, measured at 0.2 V s^{–1}, are shown in Figure 5. In the series from 11 to 15 (Table 3), the reduction potential of the diiron core becomes less negative with an overall anodic shift ($\Delta E_{1/2}$) of 330 mV. While increasing the number of carbon atoms in this series makes the reduction easier, the oxidation also becomes easier, with an overall cathodic shift (ΔE_{ox}) of 170 mV. The cathodic shift of the oxidation potential would suggest that the electron density at the diiron core has increased, but if this were the case, the reduction would become more difficult in this series. Therefore,

Table 3. Summary of the Redox Features of Complexes 11–16 in 0.1 M CH₂Cl₂/[*n*-Bu₄N][BF₄] Solution Measured at 0.2 V s^{–1} Using a Glassy Carbon Disk ($d = 1.6$ mm); Potentials *E* Are Given in Volts and Referenced to the Ferrocenium/Ferrocene (Fc⁺/Fc) Couple

complex	E_{pc} (V)	E_{pa} (V)	$E_{1/2}$ (V) ^b	E_{ox} (V)
11	–1.85	–1.62 ^a	–1.80	0.86
12	–1.85	–1.71	–1.78	0.78
13	–1.66	–1.61	–1.62	0.76
14	–1.57, –1.83	–1.50	–1.52	0.70
15	–1.54, –1.85	–	–1.47	0.69
16	–1.56, –1.87	–	–1.51	0.74

^aThis anodic event is not attributed to the oxidation of 11^{2–}. Further description of the cyclic voltammetry of 11 is given in the Supporting Information (Figure S1). ^bBecause the reduction of the complexes was irreversible or partially reversible, the $E_{1/2}$ values were estimated at the half-height of the reduction wave.

these redox reactions may be affected by reorganization processes that lead to stabilization of the electron-transfer products.^{15a} Interestingly, in going from 15 to 16, cathodic and anodic shifts in the reduction and oxidation, respectively, are observed, where $\Delta E_{1/2} = 40$ mV and $\Delta E_{\text{ox}} = 50$ mV. Thus, the complex containing six carbon atoms in the dithiolato ligand, 15, is the easiest to reduce and to oxidize in this series of complexes. One aspect of special importance for mechanistic investigation of catalytic proton reduction is the determination of the number of electrons involved in the reduction of the complex in the absence of a proton source. The reduction of diiron dithiolato complexes at the [Fe^IFe^I] redox state might occur in a stepwise two-electron-transfer fashion at E_1° and E_2° for the first and second reduction steps, respectively, where $E_1^\circ - E_2^\circ > 0$, or via transfer of two electrons at the same applied potential due to potential inversion of the two reduction steps, i.e., $E_1^\circ - E_2^\circ < 0$. It is well-established that the dependence of

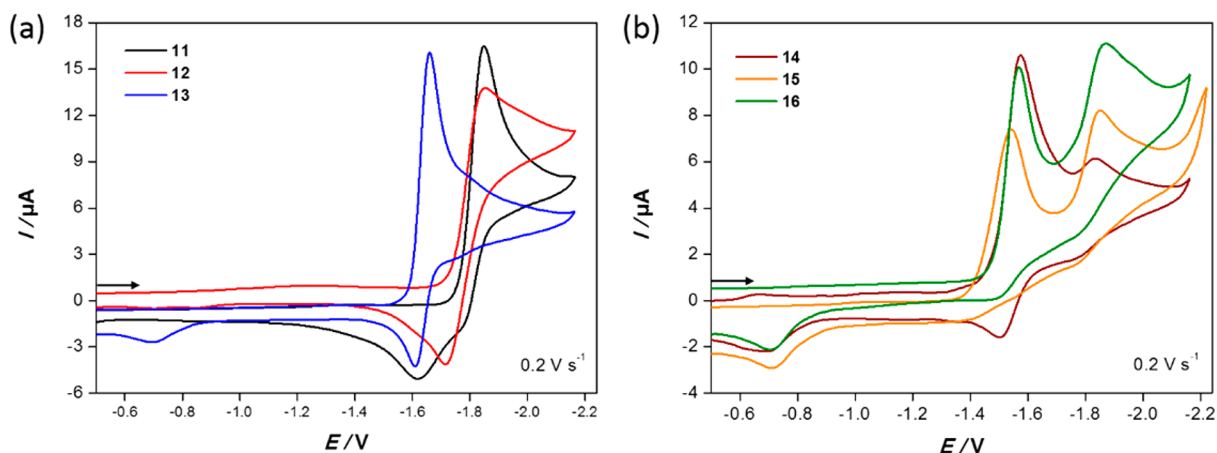


Figure 5. Cyclic voltammetry of 1.0 mM solutions of (a) complexes **11–13** and (b) complexes **14–16** in $\text{CH}_2\text{Cl}_2/[n\text{-Bu}_4\text{N}][\text{BF}_4]$ (0.1 M) at a scan rate of 0.2 V s^{-1} using a glassy carbon disk ($d = 1.6 \text{ mm}$). The potentials E are given in volts and referenced to the Fc^+/Fc couple. The arrows indicate the scan direction.

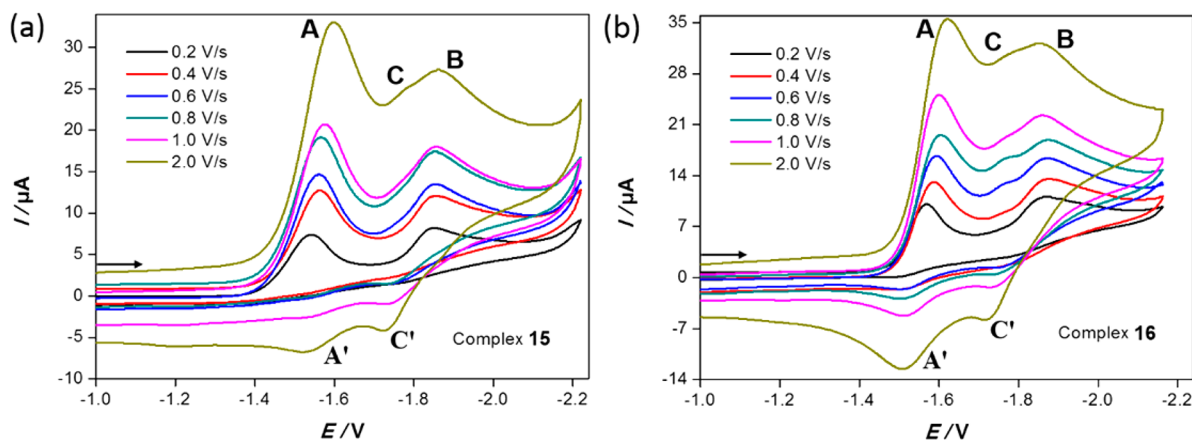


Figure 6. Cyclic voltammetry of 1.0 mM solutions of (a) complex **15** and (b) complex **16** in $\text{CH}_2\text{Cl}_2/[n\text{-Bu}_4\text{N}][\text{BF}_4]$ (0.1 M) at various scan rates using a glassy carbon disk ($d = 1.6 \text{ mm}$). The potentials E are given in volts and referenced to the Fc^+/Fc couple. The arrows indicate the scan direction.

the current function ($I_p/c \cdot \nu^{1/2} = (2.69 \times 10^5) \cdot A \cdot D^{1/2} \cdot n^{3/2}$, where I_p is the peak current, ν is the scan rate, c is the complex concentration, A is the electrode area, D is the diffusion coefficient, and n is the number of transferred electrons) on the scan rate provides mechanistic information on the electron-transfer chemistry and the number of electrons n at a given potential.^{9b,11a,c–e,g,17e,25} The scan-rate dependence of $I_p/c \cdot \nu^{1/2}$ for the first reduction of complexes **11–16** is shown in Figure S2. The value of $I_p/c \cdot \nu^{1/2}$ for the reduction peaks of complexes **11** and **13** is almost twice the magnitude of that for the other complexes, but it decreases with increasing ν toward a value predicted for a one-electron reduction, suggesting an intervening chemical process in an ECE reduction mechanism.^{9b,11a,c–e,g,17e,25} In other words, the structural change accompanying the electron transfer leads to the formation of dianionic species of **11** and **13** at a potential less negative than that required for the first electron transfer. These results are consistent with the study by Lichtenberger and co-workers,^{32a} confirming that the two-electron reduction of **11** is a consequence of a potential inversion ($E_1^0 - E_2^0 < 0$) that arises from structural changes in an ECE process. In our previous report, we discussed in detail why the value of $I_p/c \cdot \nu^{1/2}$ for the reduction of complex **12** is slightly higher than that expected for $n = 1$ and attributed that to an EC_{irr} ($E = \text{electron transfer,}$

$\text{C}_{\text{irr}} = \text{irreversible chemical reaction}$) process, where a product of the follow-up reaction is reduced at a potential closely spaced with that required to form the monoanion **12**.^{17e} In comparison, the current function of complexes **14–16** is independent of the scan rate and close to the value for $n = 1$. The cyclic voltammetry of complexes **11–13** (Figure 4a) was previously reported by us or others.^{12b,17e,32} The reduction of complex **14** (Figure 4b) is a partially reversible process at 0.2 V s^{-1} with the ratio of anodic peak current to cathodic peak current ($I_{\text{pa}}/I_{\text{pc}}$ ratio) approaching unity at higher scan rates (Figures S3 and S4a). An $I_{\text{pa}}/I_{\text{pc}}$ ratio less than 1 is a consequence of a follow-up chemical process that is prevented at high scan rates. The second reduction event of complex **14** at $E_{\text{pc}2} = -1.83 \text{ V}$ arises from species of follow-up reactions. Increasing the scan rate lowers the current of the second reduction event, which is accompanied by an increase in the $I_{\text{pa}}/I_{\text{pc}}$ ratio.^{20a,25c,33} The one-electron reduction of complexes **15** ($E_{\text{pc}1} = -1.54 \text{ V}$) and **16** ($E_{\text{pc}1} = -1.56 \text{ V}$) is an irreversible process at 0.2 V s^{-1} , as judged from reversal of the forward scans at -1.69 V (for **15**) and -1.70 V (for **16**) (see Figure S4b,c). The second irreversible reduction peaks of complexes **15** ($E_{\text{pc}2} = -1.85 \text{ V}$) and **16** ($E_{\text{pc}2} = -1.87 \text{ V}$) do not vanish when the scan rate is increased to 2.0 V s^{-1} , in contrast to the case of complex **14**. Moreover, a new reduction peak (C) starts

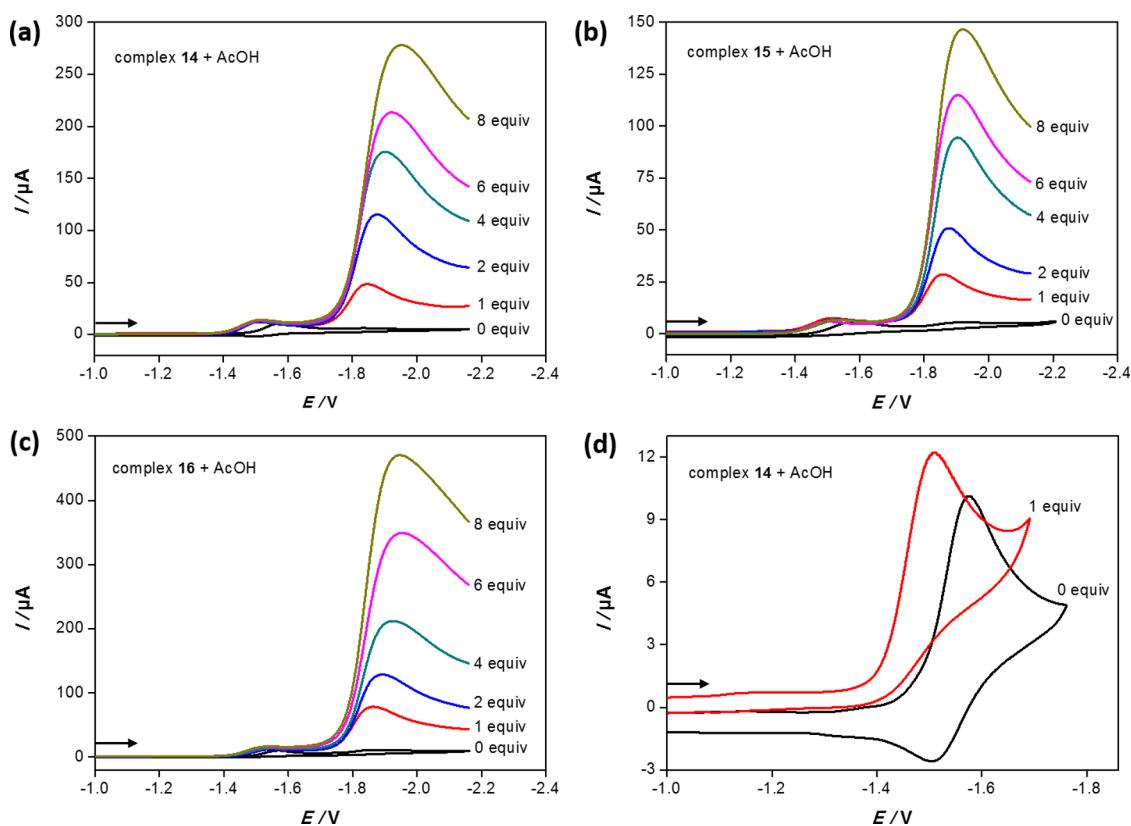


Figure 7. Cyclic voltammetry of 1.0 mM solutions of (a) complex **14**, (b) complex **15**, and (c) complex **16** in $\text{CH}_2\text{Cl}_2/[n\text{-Bu}_4\text{N}][\text{PF}_4]$ (0.1 M) at 0.2 V s^{-1} in the presence of different concentrations of AcOH using a glassy carbon disk ($d = 1.6 \text{ mm}$) and of (d) complex **15** with 1 equiv of AcOH. The arrows indicate the scan direction. The potentials E are given in V and referenced to the Fc^+/Fc couple.

to appear at $\nu \geq 2 \text{ V s}^{-1}$ ($E_{\text{pc}3} = -1.78 \text{ V}$) and $\nu \geq 0.6 \text{ V s}^{-1}$ ($E_{\text{pc}3} = -1.76 \text{ V}$) for complexes **15** and **16**, respectively (Figure 6).

The relative height of peak B with respect to A in the voltammograms of complexes **15** (Figure S5) and **16** (Figure S6) decreases as the scan rate increases. This observation is accompanied by the growth of peak C as well as the appearance of two anodic events in the return sweep, indicating enhanced reversibility of the one-electron reduction of complexes **15** and **16**. The oxidation of the monoanionic species occurs at peak A' (Figures 6, S5, and S6). These observations suggest that peak B is due to an irreversible reduction of a species formed from chemical reactions following the one-electron reduction of **15** or **16**. At high scan rates, where the follow-up reactions start to be prevented, the $\text{Fe}^{\text{I}}\text{Fe}^0/\text{Fe}^0\text{Fe}^0$ redox couple of complexes **15** and **16** is detected and indicated by C and C'.

Catalytic Reduction of Protons. The catalytic behavior of complexes **14–16** was investigated by cyclic voltammetry in the presence of various amounts of AcOH, as illustrated in Figure 7a–c. The presence of 1 equiv of AcOH in the solutions of complexes **14–16** shifts their primary reduction peaks to less negative potentials by approximately 70, 50, and 40 mV, respectively (to $E_{\text{pc}} = -1.50, -1.49, \text{ and } -1.52 \text{ V}$, respectively). This anodic shift suggests that there is an interaction between the acid and the reduced species of these complexes in CH_2Cl_2 .^{32b} As is evident from the dependence of $I_p/c\nu^{1/2}$ on the scan rate (Figure S2), these reduced species result from one-electron reduction of complexes **14–16**. Further experimental confirmation of the interaction of the acid with the monoanionic species (using complex **14** as a representative example) is shown in Figure 7d. The disappearance of the

anodic peak in the reverse scan upon addition of 1 equiv of AcOH suggests the occurrence of a chemical reaction (protonation) following the one-electron reduction of **14** in CH_2Cl_2 .^{17c} At more reducing potentials in the vicinity of -1.80 to -1.90 V for complexes **14–16**, the voltammetric profile of each complex (Figure 7a–c) shows a reduction peak with a current that increases in response to the systematic increase in the acid concentration, indicating a catalytic proton reduction. These observations suggest that the products of the EC process ($E = \text{reduction}$, $C = \text{protonation}$) for **14–16**, which occurs at ca. -1.5 V , do not lead to H_2 production unless further reduction and protonation take place at more negative potentials. For systematic comparison of the effect of the linker length on the catalytic features, we reinvestigated the behavior of complexes **11–13** in the presence of various concentrations of AcOH (data not shown in this report). Similar to complexes **14–16**, complexes **11–13** do not exhibit catalysis at their primary reduction wave but only upon application of a more negative potential. Because complexes **11** and **13** exhibit an ECE mechanism of reduction at 0.2 V s^{-1} (Figure S2), the presence of acid will lead to protonation of their dianionic species. Once the applied potential becomes sufficiently negative for subsequent reduction–protonation processes, H_2 is produced.

One property of a catalyst that describes its performance is the catalytic overpotential, which is defined in our case as the difference between the potential at half the catalytic peak current ($E_{\text{cat}/2}$) and the standard reduction potential of the acid.^{11g} A low overpotential points to an effective catalyst, which means that the catalyst operates at a potential that is close to the standard reduction potential of the acid. Because

the standard reduction potentials of acids in CH_2Cl_2 are unknown, we use the values of $E_{\text{cat}/2}$ for comparison. The catalytic potential of complex **11** ($E_{\text{cat}/2} = -2.07$ V) is ca. 300 mV more negative than those of complexes **12–16**, which in turn accomplish catalysis with comparable overpotentials reflected by $E_{\text{cat}/2} = -1.81$ V (**12**), -1.79 V (**13**), -1.77 V (**14**), -1.78 V (**15**), and -1.79 V (**16**). Another feature of the catalytic performance is the amount of current developed in response to a systematic increase in the acid concentration. The higher the current, the higher the apparent catalytic activity is. The currents for the catalytic processes of complexes **11–16** were plotted against the amount of AcOH, and the slopes were taken as a criterion of comparative catalytic activity (Figure 8).³⁴ Accordingly, complex **16** containing seven carbon atoms

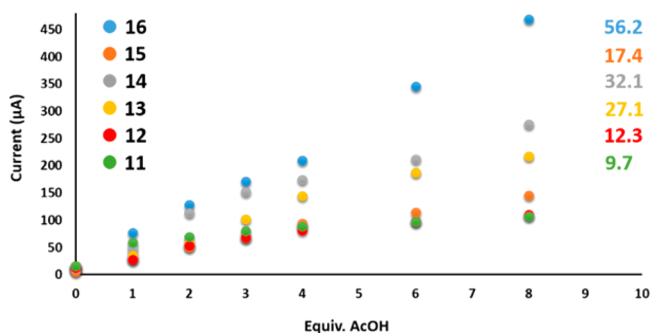


Figure 8. Dependence of the catalytic current of 1.0 mM complexes **11–16** on the amount of AcOH. The slope of each plot is given in the inset.

in the dithiolate moiety shows the greatest catalytic ability and about 6-fold higher performance compared with complex **11** containing two carbon atoms in the dithiolato ligand.

CONCLUSION

In this paper we have reported the cyclization of a series of alkyldithiols having the general formula $[\text{SH}(\text{CH}_2)_n\text{SH}]$ ($n = 4–8$) by the high-dilution technique. As a result, the monomeric, dimeric, and trimeric disulfides (**6a–10a**, **8b–10b**, and **9c**, respectively) were obtained and characterized by spectroscopic techniques as well as by X-ray structure determination in the case of **8b–10b** and **9c**. The latter compounds, with the exception of **9c**, were tested as proligands to react with $\text{Fe}_3(\text{CO})_{12}$ under different conditions in boiling THF in order to obtain complexes with the general formulas $[\text{Fe}_2(\text{CO})_6\{\mu\text{-S}(\text{CH}_2)_n\text{S}\}]$ ($n = 4–8$) (**13–17**), $[\text{Fe}_2(\text{CO})_6\{\mu\text{-S}(\text{CH}_2)_n\text{S}\}]_2$ ($n = 6–8$) (**18–20**) and $[\text{Fe}_2(\text{CO})_6\{\mu\text{-S}(\text{CH}_2)_n\text{S}\}_2]$ ($n = 6–8$) (**21–23**). Moreover, we have also reported how the physical, electrochemical, and electrocatalytic features are influenced by the systematic increase in n from 2 to 8 in complexes **11–17**. Overall, increasing the length of the linker chain of the dithiolato ligand in the all-CO complexes does not harshly change the electronic properties of the $\text{Fe}(\text{CO})_3$ units. Otherwise, the molecular structures of complexes **13–16** showed that the organic substituents are constrained to the *aa* conformation, similar to their analogous complexes **11** and **12**.^{26a,b} In contrast, the molecular structure of complex **17** exhibits an *ae* conformation, and its ^1H NMR spectrum does not show the presence of the *aa* isomer at room temperature. Therefore, to determine whether there is a dynamic interconversion between the *aa* and *ae* isomers of complex **17**, a temperature-dependent ^1H NMR experiment

was applied to a solution of complex **17** in toluene- d_8 , and we could not observe the *aa* isomer by increasing the temperature of the solution to 85 °C. The absence of the *aa* isomer in complex **17** could be explained by the short distance between the *a*- CH_2 and the sulfur atom bound to the *e*- CH_2 (3.003(2) Å) in comparison with those in complexes **13–16** (average ~ 3.694 Å). In the light of the above-mentioned considerations as well as Song's results,^{23b} we suggest that $[\text{Fe}_2(\text{CO})_6\{\mu\text{-S}(\text{CH}_2)_n\text{S}\}]$ gives only the *ae* isomer for $n \geq 8$ as a result of steric encumbrance, which is overcome for $n \leq 7$. Interestingly, the reduction and oxidation potentials of the diiron core in the systematic series from **11** to **15** are lowered with overall anodic $\Delta E_{1/2}$ and cathodic ΔE_{ox} shifts of 330 and 170 mV, respectively. Furthermore, proton reduction catalyzed by complexes **11–16** was also investigated by cyclic voltammetry in the presence of the weak acid AcOH as a proton source. It was concluded that complexes **12–16** catalyze the reduction of protons with comparable overpotentials (gauged from $E_{\text{cat}/2}$) and less negative potentials than complex **11** (ca. 300 mV). Additionally, the catalytic ability of complexes **11–16** varies in the following order: **16** > **14** > **13** > **15** > **12** > **11**.

EXPERIMENTAL SECTION

Materials and Techniques. All of the reactions were performed using standard Schlenk and vacuum-line techniques under an inert gas (nitrogen). The ^1H and $^{13}\text{C}\{^1\text{H}\}$ NMR spectra were recorded with a Bruker Avance 400 MHz spectrometer. Chemical shifts are given in parts per million with reference to internal SiMe_4 or CHCl_3 . The mass spectra were recorded with a Finnigan MAT SSQ 710 instrument. The IR spectra were recorded with a Bruker Equinox 55 spectrometer equipped with an attenuated total reflectance unit. Elemental analysis was performed with a Leco CHNS-932 apparatus. Thin-layer chromatography (TLC) was performed using Merck TLC aluminum sheets (silica gel 60 F₂₅₄). Solvents from Fisher Scientific and other chemicals from Acros and Aldrich were used without further purification. Melting points were recorded on a polarization microscope (Axiolab) connected to a heating unit (THS-600) using the software Linkam LNP and CI 93. All of the solvents were dried and distilled prior to use according to standard methods. Complexes **11** and **12** were synthesized according to the known literature methods.^{17e,32} The preparations of compounds **1–5**, **6a–10a**, **8b–10b**, and **9c** are described in detail in the Supporting Information.

Electrochemistry. Corrections for the *iR* drop were performed for all experiments. Cyclic voltammetry measurements were conducted using the three-electrode technique (glassy carbon disk (diameter $d = 1.6$ mm) as the working electrode, Ag/Ag^+ in MeCN as the reference electrode, and Pt wire as the counter electrode) with a Reference 600 potentiostat (Gamry Instruments). All of the experiments were performed in CH_2Cl_2 solution containing 0.1 M $[n\text{-Bu}_4\text{N}][\text{BF}_4]$ at room temperature; the concentration of the complexes was 1.0 mM. Solutions were deaerated by purging with N_2 for 5–10 min, and a blanket of N_2 was maintained over the solutions during the measurements. The vitreous carbon disk was polished on a felt tissue with alumina before each measurement. All of the potential values reported in this paper are referenced to the potential of the ferrocenium/ferrocene (Fc^+/Fc) couple.

Crystal Structure Determination. The intensity data for the compounds were collected on a Nonius KappaCCD diffractometer using graphite-monochromatized Mo $K\alpha$ radiation. Data were corrected for Lorentz and polarization effects; absorption was taken into account on a semiempirical basis using multiple scans.^{35–37} The structures were solved by direct methods (SHELXS³⁸) and refined by full-matrix least-squares techniques against F_o^2 (SHELXL-97³⁸). The hydrogen atoms of compounds **9c**, **15**, and **19** were included at calculated positions with fixed thermal parameters. All of the other hydrogen atoms were located by difference Fourier synthesis and refined isotropically. All non-hydrogen atoms were refined anisotropically.

cally.³⁸ The crystal of **9c** was a partial merohedral twin. The twin law was determined by PLATON³⁹ to (1.001 0.000 0.003/0.000 -1.000 0.000/-0.333 0.000 -1.001). The contribution of the main component was refined to 0.819(3). Crystallographic data as well as structure solution and refinement details are summarized in Tables S2–S4. XP (SIEMENS Analytical X-ray Instruments, Inc.) was used for structure representations.

General Procedure for the Synthesis of $[\text{Fe}_2(\text{CO})_6\{\mu\text{-S}(\text{CH}_2)_n\text{S}\}]$ ($n = 4\text{--}8$) (13–17). A solution of $\text{Fe}_3(\text{CO})_{12}$ (200 mg, 0.40 mmol) and cyclic disulfide (**6a–10a**, 0.40 mmol) in THF (30 mL) was heated at reflux for 1 h under N_2 . The green solution turned deep red, and the solvent was removed under reduced pressure. The residue was purified by column chromatography using 100% hexane. A red-orange fraction representing the complex (13–17, respectively) was collected, and the solvent was removed in vacuo. The product was obtained as a red-orange solid.

$[\text{Fe}_2(\text{CO})_6\{\mu\text{-S}(\text{CH}_2)_4\text{S}\}]$ (**13**). Yield: 60% (0.24 mmol). Mp = 113–115 °C. Anal. Calcd for $\text{C}_{10}\text{H}_8\text{Fe}_2\text{O}_6\text{S}_2$: C, 30.03; H, 2.02; S, 16.03. Found: C, 30.40; H, 2.27; S, 16.20. ^1H NMR (400 MHz, CDCl_3 , ppm): δ 2.59 (bs, 4H, SCH_2), 1.66 (bs, 4H, SCH_2CH_2). $^{13}\text{C}\{^1\text{H}\}$ NMR (100 MHz, CDCl_3 , ppm): δ 207.90 (s, CO), 33.80 (s, SCH_2), 26.09 (s, SCH_2CH_2). IR (ν_{CO} , cm^{-1}): 2072(m), 2033(vs), 1997(s). DEI-MS (m/z): 400 $[\text{M}]^+$.

$[\text{Fe}_2(\text{CO})_6\{\mu\text{-S}(\text{CH}_2)_5\text{S}\}]$ (**14**). Yield: 55% (0.22 mmol). Mp = 116–118 °C. Anal. Calcd for $\text{C}_{11}\text{H}_{10}\text{Fe}_2\text{O}_6\text{S}_2$: C, 31.91; H, 2.43; S, 15.49. Found: C, 32.31; H, 2.61; S, 15.79. ^1H NMR (400 MHz, CDCl_3 , ppm): δ 2.61 (t, 4H, SCH_2), 1.75 (p, 4H, SCH_2CH_2), 1.56 (p, 2H, $\text{SCH}_2\text{CH}_2\text{CH}_2$). $^{13}\text{C}\{^1\text{H}\}$ NMR (100 MHz, CDCl_3 , ppm): δ 207.72 (s, CO), 30.21 (s, SCH_2), 29.37 (s, SCH_2CH_2), 28.64 (s, $\text{SCH}_2\text{CH}_2\text{CH}_2$). IR (ν_{CO} , cm^{-1}): 2072(m), 2033(vs), 1999(s). DEI-MS (m/z): 414 $[\text{M}]^+$.

$[\text{Fe}_2(\text{CO})_6\{\mu\text{-S}(\text{CH}_2)_6\text{S}\}]$ (**15**). Yield: 53% (0.21 mmol). Mp = 119–121 °C. Anal. Calcd for $\text{C}_{12}\text{H}_{12}\text{Fe}_2\text{O}_6\text{S}_2$: C, 33.67; H, 2.83; S, 14.98. Found: C, 33.96; H, 3.14; S, 15.12. ^1H NMR (400 MHz, CDCl_3 , ppm): δ 2.49 (t, 4H, SCH_2), 1.64 (bs, 4H, SCH_2CH_2), 1.53 (bs, 4H, $\text{SCH}_2\text{CH}_2\text{CH}_2$). $^{13}\text{C}\{^1\text{H}\}$ NMR (100 MHz, CDCl_3 , ppm): δ 207.68 (s, CO), 32.08 (s, SCH_2), 30.52 (s, SCH_2CH_2), 26.01 (s, $\text{SCH}_2\text{CH}_2\text{CH}_2$). IR (ν_{CO} , cm^{-1}): 2072(m), 2033(vs), 1998(s). DEI-MS (m/z): 428 $[\text{M}]^+$.

$[\text{Fe}_2(\text{CO})_6\{\mu\text{-S}(\text{CH}_2)_7\text{S}\}]$ (**16**). Yield: 48% (0.19 mmol). Mp = 94–96 °C. Anal. Calcd for $\text{C}_{13}\text{H}_{14}\text{Fe}_2\text{O}_6\text{S}_2$: C, 35.32; H, 3.19; S, 14.50. Found: C, 35.72; H, 3.30; S, 14.70. ^1H NMR (400 MHz, CDCl_3 , ppm): δ 2.30 (bs, 4H, SCH_2), 1.60 (bs, 4H, SCH_2CH_2), 1.48 (bs, 4H, $\text{SCH}_2\text{CH}_2\text{CH}_2$), 1.38 (bs, 2H, $\text{SCH}_2\text{CH}_2\text{CH}_2\text{CH}_2$). $^{13}\text{C}\{^1\text{H}\}$ NMR (100 MHz, CDCl_3 , ppm): δ 207.70 (s, CO), 31.83 (s, SCH_2), 29.40 (s, SCH_2CH_2), 27.54 (s, $\text{SCH}_2\text{CH}_2\text{CH}_2$), 25.81 (s, $\text{SCH}_2\text{CH}_2\text{CH}_2\text{CH}_2$). IR (ν_{CO} , cm^{-1}): 2072(m), 2033(vs), 1994(s). DEI-MS (m/z): 442 $[\text{M}]^+$.

$[\text{Fe}_2(\text{CO})_6\{\mu\text{-S}(\text{CH}_2)_8\text{S}\}]$ (**17**). Yield: 48% (0.19 mmol). Mp = 83–85 °C. Anal. Calcd for $\text{C}_{14}\text{H}_{16}\text{Fe}_2\text{O}_6\text{S}_2$: C, 36.87; H, 3.54; S, 14.06. Found: C, 37.13; H, 3.49; S, 14.33. ^1H NMR (400 MHz, CDCl_3 , ppm): δ 2.45 (bs, 2H, $e\text{-SCH}_2$), 2.18 (bs, 2H, $a\text{-SCH}_2$), 1.87 (bs, 2H, $e\text{-SCH}_2\text{CH}_2$), 1.63 (bs, 2H, $\text{SCH}_2\text{CH}_2\text{CH}_2$), 1.54 (bs, 2H, $a\text{-SCH}_2\text{CH}_2$), 1.44 (bs, 2H, $\text{SCH}_2\text{CH}_2\text{CH}_2\text{CH}_2$), 1.34 (bs, 2H, $\text{S}(\text{CH}_2)_4\text{CH}_2$). $^{13}\text{C}\{^1\text{H}\}$ NMR (100 MHz, CDCl_3 , ppm): δ 209.17 (s, CO), 37.36 (s, $e\text{-SCH}_2$), 30.46 (s, $e\text{-SCH}_2\text{CH}_2$), 29.84 (s, $\text{SCH}_2\text{CH}_2\text{CH}_2$), 28.28 (s, $\text{SCH}_2\text{CH}_2\text{CH}_2\text{CH}_2$), 27.26 (s, $\text{S}(\text{CH}_2)_4\text{CH}_2$), 26.82 (s, $\text{S}(\text{CH}_2)_5\text{CH}_2$), 24.77 (s, $a\text{-SCH}_2\text{CH}_2$), 23.42 (s, $a\text{-SCH}_2$). IR (ν_{CO} , cm^{-1}): 2069(m), 2030(vs), 1992(s). DEI-MS (m/z): 456 $[\text{M}]^+$.

General Procedure for the Synthesis of Complexes 18–20 via Reaction of Compounds 8b–10b with $\text{Fe}_3(\text{CO})_{12}$ in a 1:2 Molar Ratio. A solution of $\text{Fe}_3(\text{CO})_{12}$ (400 mg, 0.80 mmol) and cyclic tetrasulfide (**8b–10b**, 0.40 mmol) in THF (40 mL) was heated at reflux for 2 h under N_2 . The green solution turned deep red, and the solvent was removed under reduced pressure. The residue was purified by column chromatography using 100% hexane. A red-orange fraction representing the complex (18–20, respectively) was collected, and the solvent was removed in vacuo. The product was obtained as a red-orange solid.

$[\text{Fe}_2(\text{CO})_6\{\mu\text{-S}(\text{CH}_2)_6\text{S}\}]_2$ (**18**). Yield: 33% (0.13 mmol). Mp = 210–211 °C. Anal. Calcd for $\text{C}_{24}\text{H}_{24}\text{Fe}_4\text{O}_{12}\text{S}_4$: C, 33.67; H, 2.83; S, 14.98. Found: C, 33.99; H, 3.10; S, 15.20. ^1H NMR (400 MHz, CDCl_3 , ppm): δ 2.46 (bs, 4H, $e\text{-SCH}_2$), 2.13 (bs, 4H, $a\text{-SCH}_2$), 1.62 (bs, 8H, SCH_2CH_2), 1.48 (bs, 8H, $\text{SCH}_2\text{CH}_2\text{CH}_2$). $^{13}\text{C}\{^1\text{H}\}$ NMR (100 MHz, CDCl_3 , ppm): δ 208.97 (s, CO), 39.05 (s, $e\text{-SCH}_2$), 32.68, 31.41, 28.76, 26.42, 23.84 (s, $a\text{-SCH}_2$). IR (ν_{CO} , cm^{-1}): 2068(m), 2033(vs), 1991(s). DEI-MS (m/z): 856 $[\text{M}]^+$.

$[\text{Fe}_2(\text{CO})_6\{\mu\text{-S}(\text{CH}_2)_7\text{S}\}]_2$ (**19**). Yield: 25% (0.10 mmol). Mp = 102–103 °C. Anal. Calcd for $\text{C}_{26}\text{H}_{28}\text{Fe}_4\text{O}_{12}\text{S}_4$: C, 35.32; H, 3.19; S, 14.50. Found: C, 35.62; H, 3.38; S, 14.67. ^1H NMR (400 MHz, CDCl_3 , ppm): δ 2.47 (bs, 4H, $e\text{-SCH}_2$), 2.08 (bs, 4H, $a\text{-SCH}_2$), 1.75–1.59 (m, 8H, SCH_2CH_2), 1.46–1.26 (m, 12H, $\text{SCH}_2\text{CH}_2(\text{CH}_2)_2$). $^{13}\text{C}\{^1\text{H}\}$ NMR (100 MHz, CDCl_3 , ppm): δ 208.97 (s, CO), 39.04 (s, $e\text{-SCH}_2$), 32.68, 31.41, 28.76, 26.42, 23.84 (s, $a\text{-SCH}_2$). IR (ν_{CO} , cm^{-1}): 2068(m), 2033(vs), 1990(s). DEI-MS (m/z): 884 $[\text{M}]^+$.

$[\text{Fe}_2(\text{CO})_6\{\mu\text{-S}(\text{CH}_2)_8\text{S}\}]_2$ (**20**). Yield: 30% (0.12 mmol). Mp = 165–166 °C. Anal. Calcd for $\text{C}_{28}\text{H}_{32}\text{Fe}_4\text{O}_{12}\text{S}_4$: C, 36.87; H, 3.54; S, 14.06. Found: C, 37.20; H, 3.65; S, 14.31. ^1H NMR (400 MHz, CDCl_3 , ppm): δ 2.44 (bs, 4H, $e\text{-SCH}_2$), 2.11 (bs, 4H, $a\text{-SCH}_2$), 1.67 (bs, 8H, SCH_2CH_2), 1.52 (bs, 8H, $\text{SCH}_2\text{CH}_2\text{CH}_2$), 1.44 (bs, 4H, $\text{S}(\text{CH}_2)_3\text{CH}_2$), 1.31 (bs, 4H, $\text{S}(\text{CH}_2)_4\text{CH}_2$). $^{13}\text{C}\{^1\text{H}\}$ NMR (100 MHz, CDCl_3 , ppm): δ 209.04 (s, CO), 39.37 (s, $e\text{-SCH}_2$), 32.96, 31.93, 29.12, 28.95, 28.42, 28.01, 24.64 (s, $a\text{-SCH}_2$). IR (ν_{CO} , cm^{-1}): 2068(m), 2032(vs), 1991(s). DEI-MS (m/z): 912 $[\text{M}]^+$, 884 $[\text{M} - \text{CO}]^+$, 856 $[\text{M} - 2\text{CO}]^+$, 828 $[\text{M} - 3\text{CO}]^+$, 800 $[\text{M} - 4\text{CO}]^+$, 772 $[\text{M} - 5\text{CO}]^+$, 744 $[\text{M} - 6\text{CO}]^+$, 716 $[\text{M} - 7\text{CO}]^+$, 688 $[\text{M} - 8\text{CO}]^+$, 660 $[\text{M} - 9\text{CO}]^+$, 632 $[\text{M} - 10\text{CO}]^+$, 604 $[\text{M} - 11\text{CO}]^+$, 576 $[\text{M} - 12\text{CO}]^+$.

General Procedure for the Synthesis of Complexes 21–23 via Reaction of Compounds 8b–10b with $\text{Fe}_3(\text{CO})_{12}$ in a 1:1 Molar Ratio. A solution of $\text{Fe}_3(\text{CO})_{12}$ (100 mg, 0.20 mmol) and cyclic tetrasulfide (**8b–10b**, 0.20 mmol) in THF (40 mL) was heated at reflux for 2 h under N_2 . The green solution turned deep red, and the solvent was removed under reduced pressure. The residue was purified by column chromatography using 100% hexane. A yellow-orange fraction representing the complex (21–23, respectively) was collected, and the solvent was removed in vacuo. The product was obtained as a red-orange solid.

$[\text{Fe}_2(\text{CO})_6\{\mu\text{-S}(\text{CH}_2)_6\text{S}\}]$ (**21**). Yield: 15% (0.030 mmol). Mp = 170–171 °C. Anal. Calcd for $\text{C}_{18}\text{H}_{24}\text{Fe}_2\text{O}_6\text{S}_4$: C, 37.51; H, 4.20; S, 22.25. Found: C, 37.26; H, 4.03; S, 21.96. ^1H NMR (400 MHz, CDCl_3 , ppm): δ 2.71 (bs, 4H, SSCH_2), 2.51 (bs, 2H, $e\text{-SCH}_2$), 2.14 (bs, 2H, $a\text{-SCH}_2$), 1.72 (bs, 4H, SSCH_2CH_2), 1.43 (bs, 4H, SCH_2CH_2), 1.27 (bs, 8H, $\text{S}(\text{CH}_2)_2(\text{CH}_2)_2$). IR (ν_{CO} , cm^{-1}): 2069(m), 2031(vs), 1992(s). DEI-MS (m/z): 576 $[\text{M}]^+$.

$[\text{Fe}_2(\text{CO})_6\{\mu\text{-S}(\text{CH}_2)_7\text{S}\}]$ (**22**). Yield: 10% (0.020 mmol). Mp = 73–75 °C. Anal. Calcd for $\text{C}_{20}\text{H}_{28}\text{Fe}_2\text{O}_6\text{S}_4$: C, 39.75; H, 4.67; S, 21.22. Found: C, 39.95; H, 4.48; S, 21.46. ^1H NMR (400 MHz, CDCl_3 , ppm): δ 2.75 (bs, 4H, SSCH_2), 2.50 (bs, 2H, $e\text{-SCH}_2$), 2.11 (bs, 2H, $a\text{-SCH}_2$), 1.73 (bs, 4H, SSCH_2CH_2), 1.46 (bs, 4H, SCH_2CH_2), 1.33–1.29 (m, 12H, $\text{S}(\text{CH}_2)_2(\text{CH}_2)_2$). IR (ν_{CO} , cm^{-1}): 2069(m), 2032(vs), 1991(s). DEI-MS (m/z): 604 $[\text{M}]^+$.

$[\text{Fe}_2(\text{CO})_6\{\mu\text{-S}(\text{CH}_2)_8\text{S}\}]$ (**23**). Yield: 12% (0.024 mmol). Mp = 122–123 °C. Anal. Calcd for $\text{C}_{22}\text{H}_{32}\text{Fe}_2\text{O}_6\text{S}_4$: C, 41.78; H, 5.10; S, 20.28. Found: C, 41.48; H, 5.32; S, 19.99. ^1H NMR (400 MHz, CDCl_3 , ppm): δ 2.72 (bs, 4H, SSCH_2), 2.52 (bs, 2H, $e\text{-SCH}_2$), 2.15 (bs, 2H, $a\text{-SCH}_2$), 1.70 (bs, 4H, SSCH_2CH_2), 1.45 (bs, 4H, SCH_2CH_2), 1.40 (bs, 8H, $\text{SCH}_2\text{CH}_2\text{CH}_2$), 1.39 (bs, 4H, $\text{S}(\text{CH}_2)_3\text{CH}_2$), 1.30 (bs, 4H, $\text{S}(\text{CH}_2)_4\text{CH}_2$). IR (ν_{CO} , cm^{-1}): 2069(m), 2030(vs), 1991(s). DEI-MS (m/z): 632 $[\text{M}]^+$.

■ ASSOCIATED CONTENT

Supporting Information

The Supporting Information is available free of charge on the ACS Publications website at DOI: 10.1021/acs.inorgchem.7b01398.

General experimental details, cyclic voltammetry of complex **11** in CH₂Cl₂, Figures S1–S6, and Tables S1–S4 (PDF)

Accession Codes

CCDC 1546654–1546666 contain the supplementary crystallographic data for this paper. These data can be obtained free of charge via www.ccdc.cam.ac.uk/data_request/cif, or by emailing data_request@ccdc.cam.ac.uk, or by contacting The Cambridge Crystallographic Data Centre, 12 Union Road, Cambridge CB2 1EZ, U.K.; fax: +44 1223 336033.

AUTHOR INFORMATION

Corresponding Author

*E-mail: wolfgang.weigand@uni-jena.de.

ORCID

Hassan Abul-Futouh: 0000-0003-2419-9782

Wolfgang Weigand: 0000-0001-5177-1006

Notes

The authors declare no competing financial interest.

ACKNOWLEDGMENTS

H.A.-F. thanks the Deutscher Akademischer Austausch Dienst (DAAD) for a scholarship. We are grateful to Dr. Manfred Rudolph for valuable discussions.

DEDICATION

Dedicated to Prof. Marian Mikolajczyk on the occasion of his 80th birthday.

REFERENCES

- (1) Wuebbles, D. J.; Jain, A. K. Concerns About Climate Change and the Role of Fossil Fuel Use. *Fuel Process. Technol.* **2001**, *71*, 99–119.
- (2) (a) Koroneos, C.; Dompros, A.; Roumbas, G.; Moussiopoulos, N. Life Cycle Assessment of Hydrogen Fuel Production Processes. *Int. J. Hydrogen Energy* **2004**, *29*, 1443–1450. (b) Hignett, T. P. *Fertilizers Manual*; Springer: Dordrecht, The Netherlands, 1985. (c) Rauche, H. *Die Kaliindustrie im 21 Jahrhundert*; Springer: Berlin, 2015.
- (3) Borup, R.; Meyers, J.; Pivovar, B.; Kim, Y. S.; Mukundan, R.; Garland, N.; Myers, D.; Wilson, M.; Garzon, F.; Wood, D.; Zelenay, P.; More, K.; Stroh, K.; Zawodzinski, T.; Boncella, J.; McGrath, J. E.; Inaba, M.; Miyatake, K.; Hori, M.; Ota, K.; Ogumi, Z.; Miyata, S.; Nishikata, A.; Siroma, Z.; Uchimoto, Y.; Yasuda, K.; Kimijima, K. I.; Iwashita, N. Scientific Aspects of Polymer Electrolyte Fuel Cell Durability and Degradation. *Chem. Rev.* **2007**, *107*, 3904–3951.
- (4) (a) Adams, M. W. The Structure and Mechanism of Iron-Hydrogenases. *Biochim. Biophys. Acta, Bioenerg.* **1990**, *1020*, 115–145. (b) Frey, M. Hydrogenases: Hydrogen-Activating Enzyme. *Chem-BioChem* **2002**, *3*, 153–160. (c) Evans, D. J.; Pickett, C. J. Chemistry and the Hydrogenases. *Chem. Soc. Rev.* **2003**, *32*, 268–275. (d) Volbeda, A.; Fontecilla-Camps, J. C. Structure-Function Relationships of Nickel-Iron Sites in Hydrogenase and a Comparison with the Active Sites of Other Nickel-Iron Enzymes. *Coord. Chem. Rev.* **2005**, *249*, 1609–1619.
- (5) Fontecilla-Camps, J. C.; Volbeda, A.; Cavazza, C.; Nicolet, Y. Structure/Function Relationships of [NiFe]- and [FeFe]-Hydrogenases. *Chem. Rev.* **2007**, *107*, 4273–4303.
- (6) Lubitz, W.; Ogata, H.; Rüdiger, O.; Reijerse, E. Hydrogenases. *Chem. Rev.* **2014**, *114*, 4081–4148.
- (7) (a) Adamska-Venkatesh, A.; Roy, S.; Siebel, J. F.; Simmons, T. R.; Fontecave, M.; Artero, V.; Reijerse, E.; Lubitz, W. Spectroscopic Characterization of the Bridging Amine in the Active Site of [FeFe] Hydrogenase Using Isotopologues of the H-Cluster. *J. Am. Chem. Soc.* **2015**, *137*, 12744–12747. (b) Adamska, A.; Silakov, A.; Lambert, C.; Rüdiger, O.; Happe, T.; Reijerse, E.; Lubitz, W. Identification

and Characterization of the “Super-Reduced” State of the H-Cluster in [FeFe] Hydrogenase: A New Building Block for the Catalytic Cycle? *Angew. Chem., Int. Ed.* **2012**, *51*, 11458–11462. (c) Fan, H.-J.; Hall, M. B. A Capable Bridging Ligand for Fe-Only Hydrogenase: Density Functional Calculations of a Low-Energy Route for Heterolytic Cleavage and Formation of Dihydrogen. *J. Am. Chem. Soc.* **2001**, *123*, 3828–3829. (d) Peters, J. W.; Lanzilotta, W. N.; Lemon, B. J.; Seefeldt, L. C. X-ray Crystal Structure of the Fe-Only Hydrogenase (CpI) from *Clostridium pasteurianum* to 1.8 Å Resolution. *Science* **1998**, *282*, 1853–1858. (e) Nicolet, Y.; de Lacey, A. L.; Vernede, X.; Fernandez, V. M.; Hatchikian, E. C.; Fontecilla-Camps, J. C. Crystallographic and FTIR Spectroscopic Evidence of Changes in Fe Coordination Upon Reduction of the Active Site of the Fe-Only Hydrogenase from *Desulfovibrio desulfuricans*. *J. Am. Chem. Soc.* **2001**, *123*, 1596–1601. (f) Reijerse, E. J.; Pham, C. C.; Pelmenschikov, V.; Gilbert-Wilson, R.; Adamska-Venkatesh, A.; Siebel, J. F.; Gee, L. B.; Yoda, Y.; Tamasaku, K.; Lubitz, W.; Rauchfuss, T. B.; Cramer, S. P. Direct Observation of an Iron-Bound Terminal Hydride in [FeFe]-Hydrogenase by Nuclear Resonance Vibrational Spectroscopy. *J. Am. Chem. Soc.* **2017**, *139*, 4306–4309.

(8) Li, Y.; Rauchfuss, T. B. Synthesis of Diiron(I) Dithiolate Carbonyl Complexes. *Chem. Rev.* **2016**, *116*, 7043–7077 and references cited therein.

(9) (a) Wright, R. J.; Lim, C.; Tilley, T. D. Diiron Proton Reduction Catalysts Possessing Electron-Rich and Electron-Poor Naphthalene-1,8-dithiolate Ligands. *Chem. - Eur. J.* **2009**, *15*, 8518–8525. (b) Qian, G.; Zhong, W.; Wei, Z.; Wang, H.; Xiao, Z.; Long, L.; Liu, X. Diiron Hexacarbonyl Complexes Bearing Naphthalene-1,8-Dithiolate Bridge Moiety as Mimics of the Sub-Unit of [FeFe]-Hydrogenase: Synthesis, Characterisation and Electrochemical Investigations. *New J. Chem.* **2015**, *39*, 9752–9760. (c) Figliola, C.; Male, L.; Horton, P. N.; Pitak, M. B.; Coles, S. J.; Horswell, S. L.; Grainger, R. S. [FeFe]-Hydrogenase Synthetic Mimics Based on Peri-Substituted Dichalcogenides. *Organometallics* **2014**, *33*, 4449–4460. (d) Figliola, C.; Male, L.; Horswell, S. L.; Grainger, R. S. N-Derivatives of Peri-Substituted Dichalcogenide [FeFe]-Hydrogenase Mimics: Towards Photocatalytic Dyads for Hydrogen Production. *Eur. J. Inorg. Chem.* **2015**, *2015*, 3146–3156. (e) Topf, C.; Monkowius, U.; Knör, G. Design, Synthesis and Characterization of a Modular Bridging Ligand Platform for Bio-Inspired Hydrogen Production. *Inorg. Chem. Commun.* **2012**, *21*, 147–150. (f) Mebi, C. A.; Noll, B. C.; Gao, R.; Karr, D. Binuclear Iron(I) Complex Containing Bridging Phenanthrene-4,5-dithiolate Ligand: Preparation, Spectroscopy, Crystal Structure, and Electrochemistry. *Z. Anorg. Allg. Chem.* **2010**, *636*, 2550–2554. (g) Abul-Futouh, H.; Zagranjarski, Y.; Müller, C.; Schulz, M.; Kupfer, S.; Görls, H.; El-khateeb, M.; Gräfe, S.; Dietzek, B.; Peneva, K.; Weigand, W. [FeFe]-Hydrogenase H-cluster Mimics Mediated by Naphthalene Monoimide Derivatives of Peri-Substituted Dichalcogenides. *Dalton Trans.* **2017**, DOI: 10.1039/C7DT02079A.

(10) (a) Samuel, A. P. S.; Co, D. T.; Stern, C. L.; Wasielewski, M. R. Ultrafast Photodriven Intramolecular Electron Transfer from a Zinc Porphyrin to a Readily Reduced Diiron Hydrogenase Model Complex. *J. Am. Chem. Soc.* **2010**, *132*, 8813–8815. (b) Li, P.; Amirjalayer, S.; Hartl, F.; Lutz, M.; Bruin, B.; Becker, R.; Woutersen, S.; Reek, J. N. H. Direct Probing of Photoinduced Electron Transfer in a Self-Assembled Biomimetic [2Fe2S]-Hydrogenase Complex Using Ultrafast Vibrational Spectroscopy. *Inorg. Chem.* **2014**, *53*, 5373–5383.

(11) (a) Gloaguen, F.; Morvan, D.; Capon, J.-F.; Schollhammer, P.; Talarmin, J. Electrochemical Proton Reduction at Mild Potentials by Monosubstituted Diiron Organometallic Complexes Bearing a Benzenedithiolate Bridge. *J. Electroanal. Chem.* **2007**, *603*, 15–20. (b) Felton, G. A. N.; Vannucci, A. K.; Chen, J.; Lockett, L. T.; Okumura, N.; Petro, B. J.; Zakai, U. I.; Evans, D. H.; Glass, R. S.; Lichtenberger, D. L. Hydrogen Generation from Weak Acids: Electrochemical and Computational Studies of a Diiron Hydrogenase Mimic. *J. Am. Chem. Soc.* **2007**, *129*, 12521–12530. (c) Schwartz, L.; Singh, P. S.; Eriksson, L.; Lomoth, R.; Ott, S. Tuning the Electronic Properties of Fe₂(μ-Arenedithiolate)(CO)_{6-n}(PMe₃)_n (n = 0, 2) Complexes Related to the [Fe–Fe]-Hydrogenase Active Site. *C. R.*

Chim. **2008**, *11*, 875–889. (d) Capon, J.-F.; Gloaguen, F.; Schollhammer, P.; Talarmin, J. Electrochemical Proton Reduction by Thiolate-Bridged Hexacarbonyl Diiron Clusters. *J. Electroanal. Chem.* **2004**, *566*, 241–247. (e) Chen, J.; Vannucci, A. K.; Mebi, C. A.; Okumura, N.; Borowski, S. C.; Swenson, M.; Lockett, L. T.; Evans, D. H.; Glass, R. S.; Lichtenberger, D. L. Synthesis of Diiron Hydrogenase Mimics Bearing Hydroquinone and Related Ligands. Electrochemical and Computational Studies of the Mechanism of Hydrogen Production and the Role of O–H...S Hydrogen Bonding. *Organometallics* **2010**, *29*, 5330–5340. (f) Donovan, E. S.; McCormick, J. J.; Nichol, G. S.; Felton, G. A. N. Cyclic Voltammetric Studies of Chlorine-Substituted Diiron Benzenedithiolato Hexacarbonyl Electrocatalysts Inspired by the [FeFe]-Hydrogenase Active Site. *Organometallics* **2012**, *31*, 8067–8070. (g) Felton, G. A. N.; Mebi, C. A.; Petro, B. J.; Vannucci, A. K.; Evans, D. H.; Glass, R. S.; Lichtenberger, D. L. Review of Electrochemical Studies of Complexes Containing the [Fe₂S₂] Core Characteristic of [FeFe]-Hydrogenases Including Catalysis by These Complexes of the Reduction of Acids to Form Dihydrogen. *J. Organomet. Chem.* **2009**, *694*, 2681–2699.

(12) (a) Lawrence, J. D.; Li, H. X.; Rauchfuss, T. B.; Benard, M.; Rohmer, M. M. Diiron Azadithiolates as Models for the Iron-Only Hydrogenase Active Site: Synthesis, Structure, and Stereoelectronics. *Angew. Chem., Int. Ed.* **2001**, *40*, 1768–1771. (b) Capon, J.-F.; Ezzaher, S.; Gloaguen, F.; Pétilion, F. Y.; Schollhammer, P.; Talarmin, J.; Davin, T. J.; McGrady, J. E.; Muir, K. W. Electrochemical and Theoretical Investigations of the Reduction of [Fe₂(CO)₃L(μ-SCH₂XCH₂S)] Complexes Related to [FeFe] Hydrogenase. *New J. Chem.* **2007**, *31*, 2052–2064. (c) Wang, F.; Wang, M.; Liu, X.; Jin, K.; Dong, W.; Sun, L. Protonation, Electrochemical Properties and Molecular Structures of Halogen-Functionalized Diiron Azadithiolate Complexes Related to the Active Site of Iron-Only Hydrogenases. *Dalton Trans.* **2007**, 3812–3819. (d) Cui, H.-G.; Wang, M.; Dong, W.-B.; Duan, L.-L.; Li, P.; Sun, L.-C. Synthesis, Structures and Electrochemical Properties of Hydroxyl- and Pyridyl-Functionalized Diiron Azadithiolate Complexes. *Polyhedron* **2007**, *26*, 904–910. (e) Jiang, S.; Liu, J.; Sun, A. Furan-Containing Diiron Azadithiolate Hexacarbonyl Complex with Unusual Lower Catalytic Proton Reduction Potential. *Inorg. Chem. Commun.* **2006**, *9*, 290–292. (f) Wang, Z.; Liu, J.-H.; He, C.-J.; Jiang, S.; Åkermark, B.; Sun, L.-C. Azadithiolates Cofactor of the Iron-Only Hydrogenase and its PR₃-Monosubstituted Derivatives: Synthesis, Structure, Electrochemistry and Protonation. *J. Organomet. Chem.* **2007**, *692*, 5501–5507. (g) Wang, W.-G.; Wang, H.-Y.; Si, G.; Tung, C.-H.; Wu, L.-Z. Fluorophenyl-Substituted Fe-Only Hydrogenases Active Site ADT Models: Different Electrocatalytic Process for Proton Reduction in HOAc and HBF₄/Et₂O. *Dalton Trans.* **2009**, 2712–2720. (h) Na, Y.; Wang, M.; Pan, J.; Zhang, P.; Åkermark, B.; Sun, L. Visible Light-Driven Electron Transfer and Hydrogen Generation Catalyzed by Bioinspired [2Fe₂S] Complexes. *Inorg. Chem.* **2008**, *47*, 2805–2810. (i) Wang, Z.; Liu, J.; He, C.; Jiang, S.; Åkermark, B.; Sun, L. Diiron Azadithiolates with Hydrophilic Phosphatridiazadamantane Ligand as Iron-Only Hydrogenase Active Site Models: Synthesis, Structure, and Electrochemical Study. *Inorg. Chim. Acta* **2007**, *360*, 2411–2419. (j) Si, Y.; Ma, C.; Hu, M.; Chen, H.; Chen, C.; Liu, Q. (N-C_nH_{2n-1})-1,3-Azapropandithiolate (n = 5, 6, 7)-Bridged Diiron Complexes as Mimics for the Active Site of [FeFe]-Hydrogenases: The Influence of the Bridge on the Diiron Complex. *New J. Chem.* **2007**, *31*, 1448–1454. (k) Schwartz, L.; Eilers, G.; Eriksson, L.; Gogoll, A.; Lomoth, R.; Ott, S. Iron Hydrogenase Active Site Mimic Holding a Proton and a Hydride. *Chem. Commun.* **2006**, 520–526. (l) Eilers, G.; Schwartz, L.; Stein, M.; Zampella, G.; De Gioia, L.; Ott, S.; Lomoth, R. Ligand versus Metal Protonation of an Iron Hydrogenase Active Site Mimic. *Chem. - Eur. J.* **2007**, *13*, 7075–7084. (m) Hou, J.; Peng, X.; Liu, J.; Gao, Y.; Zhao, X.; Gao, S.; Han, K. A Binuclear Isocyanide Azadithiolatoiron Complex Relevant to the Active Site of Fe-Only Hydrogenases: Synthesis, Structure and Electrochemical Properties. *Eur. J. Inorg. Chem.* **2006**, *2006*, 4679–4686. (n) Ezzaher, S.; Orain, P.-Y.; Capon, J.-F.; Gloaguen, F.; Pétilion, F. Y.; Roisnel, T.; Schollhammer, P.; Talarmin, J. First Insights Into the Protonation of Dissymmetrically Disubstituted Di-Iron

Azadithiolate Models of the [FeFe]H₂ases Active Site. *Chem. Commun.* **2008**, 2547–2549. (o) Carroll, M. E.; Barton, B. E.; Rauchfuss, T. B.; Carroll, J. P. Synthetic Models for the Active Site of the [FeFe]-Hydrogenase: Catalytic Proton Reduction and the Structure of the Doubly Protonated Intermediate. *J. Am. Chem. Soc.* **2012**, *134*, 18843–18852.

(13) (a) Zaffaroni, R.; Rauchfuss, T. B.; Gray, D. L.; De Gioia, L.; Zampella, G. Terminal vs Bridging Hydrides of Diiron Dithiolates: Protonation of Fe₂(dithiolate)(CO)₂(PMe₃)₄. *J. Am. Chem. Soc.* **2012**, *134*, 19260–19269. (b) Winter, A.; Zsolnai, L.; Huttner, G. Deprotonierung und Substitutionsreaktionen Dreikerniger Eisencluster Fe₃(CO)₉(H)(SR). *Chem. Ber.* **1982**, *115*, 1286–1304. (c) Winter, A.; Zsolnai, L.; Huttner, G. Dinuclear and Trinuclear Carbonyliron Complexes Containing 1,2- and 1,3-Dithiolato Bridging Ligands. *Z. Naturforsch., B: J. Chem. Sci.* **1982**, *37*, 1430–1436. (d) Singleton, M. L.; Jenkins, R. M.; Klemashevich, C. L.; Darensbourg, M. Y. The Effect of Bridgehead Steric Bulk on the Ground State and Intramolecular Exchange Processes of (μ-SCH₂CR₂CH₂S)[Fe(CO)₃][Fe(CO)₂L] Complexes. *C. R. Chim.* **2008**, *11*, 861–874. (e) Barton, B. E.; Olsen, M. T.; Rauchfuss, T. B. Aza- and Oxadithiolates Are Probable Proton Relays in Functional Models for the [FeFe]-Hydrogenases. *J. Am. Chem. Soc.* **2008**, *130*, 16834–16835. (f) Barton, B. E.; Rauchfuss, T. B. Terminal Hydride in [FeFe]-Hydrogenase Model Has Lower Potential for H₂ Production Than the Isomeric Bridging Hydride. *Inorg. Chem.* **2008**, *47*, 2261–2263. (g) Trautwein, R.; Almazahreh, L. R.; Görls, H.; Weigand, W. The Influence of OH Groups in [Fe(CO)₃]₂(μ-ECH₂)₂C(CH₂OH)₂ (E = S, Se) Complexes Toward the Cathodic Process. *Z. Anorg. Allg. Chem.* **2013**, *639*, 1512–1519.

(14) (a) Goy, R.; Bertini, L.; Görls, H.; De Gioia, L.; Talarmin, J.; Zampella, G.; Schollhammer, P.; Weigand, W. Silicon-Heteroaromatic [FeFe] Hydrogenase Model Complexes: Insight into Protonation, Electrochemical Properties, and Molecular Structures. *Chem. - Eur. J.* **2015**, *21*, 5061–5073. (b) Apfel, U.-P.; Troegel, D.; Halpin, Y.; Tschierlei, S.; Uhlemann, U.; Görls, H.; Schmitt, M.; Popp, J.; Dunne, P.; Venkatesan, M.; Coey, M.; Rudolph, M.; Vos, G. J.; Tacke, R.; Weigand, W. Models for the Active Site in [FeFe] Hydrogenase with Iron-Bound Ligands Derived from Bis-, Tris-, and Tetrakis(mercaptomethyl)silanes. *Inorg. Chem.* **2010**, *49*, 10117–10132.

(15) (a) Abul-Futouh, H.; Almazahreh, L. R.; Sakamoto, T.; Stessman, N. Y. T.; Lichtenberger, D. L.; Glass, R. S.; Görls, H.; El-khateeb, M.; Schollhammer, P.; Mloston, G.; Weigand, W. [FeFe]-Hydrogenase H-Cluster Mimics with Unique Planar μ-(SCH₂)₂ER₂ Linkers (E = Ge and Sn). *Chem. - Eur. J.* **2017**, *23*, 346–359. (b) Glass, R. S.; Gruhn, N. E.; Lorange, E.; Singh, M. S.; Stessman, N. Y. T.; Zakai, U. I. Synthesis, Gas-Phase Photoelectron Spectroscopic, and Theoretical Studies of Stannylated Dinuclear Iron Dithiolates. *Inorg. Chem.* **2005**, *44*, 5728–5737.

(16) Almazahreh, L. R.; Apfel, U.-P.; Imhof, W.; Rudolph, M.; Görls, H.; Talarmin, J.; Schollhammer, P.; El-khateeb, M.; Weigand, W. A Novel [FeFe] Hydrogenase Model with a (SCH₂)₂P=O Moiety. *Organometallics* **2013**, *32*, 4523–4530.

(17) (a) Harb, M. K.; Windhager, J.; Niksch, T.; Görls, H.; Sakamoto, T.; Smith, E. R.; Glass, R. S.; Lichtenberger, D. L.; Evans, D. H.; El-khateeb, M.; Weigand, W. Comparison of S and Se Dichalcogenolato [FeFe]-Hydrogenase Models with Central S and Se Atoms in the Bridgehead Chain. *Tetrahedron* **2012**, *68*, 10592–10599. (b) Gao, S.; Fan, J.; Sun, S.; Peng, X.; Zhao, X.; Hou, J. Selenium-Bridged Diiron Hexacarbonyl Complexes as Biomimetic Models for the Active site of Fe–Fe Hydrogenases. *Dalton Trans.* **2008**, 2128–2135. (c) Harb, M. K.; Apfel, U.-P.; Kübel, J.; Görls, H.; Felton, G. A. N.; Sakamoto, T.; Evans, D. H.; Glass, R. S.; Lichtenberger, D. L.; El-khateeb, M.; Weigand, W. Preparation and Characterization of Homologous Diiron Dithiolato, Diselenato, and Ditellurato Complexes: [FeFe]-Hydrogenase Models. *Organometallics* **2009**, *28*, 6666–6675. (d) Abul-Futouh, H.; El-khateeb, M.; Görls, H.; Asali, K. J.; Weigand, W. Selenium Makes the Difference: Protonation of [FeFe]-Hydrogenase Mimics with Diselenolato Ligands. *Dalton Trans.* **2017**, *46*, 2937–2947. (e) Trautwein, R.; Almazahreh, L. R.; Görls, H.;

Weigand, W. Steric Effect of the Dithiolato Linker on the Reduction Mechanism of $[\text{Fe}_2(\text{CO})_6\{\mu-(\text{XCH}_2)_2\text{CRR}'\}]$ Hydrogenase Models (X = S, Se). *Dalton Trans.* **2015**, *44*, 18780–18794. (f) Gao, W.; Song, L.-C.; Yin, B.-S.; Zan, H.-N.; Wang, D.-F.; Song, H.-B. Synthesis and Characterization of Single, Double, and Triple Butterfly $[2\text{Fe}_2\text{E}]$ (E = Se, S) Cluster Complexes Related to the Active Site of $[\text{FeFe}]$ -Hydrogenases. *Organometallics* **2011**, *30*, 4097–4107. (g) Song, L.-C.; Gao, W.; Feng, C.-P.; Wang, D.-F.; Hu, Q.-M. Investigations on Synthesis, Structure, and Properties of New Butterfly $[2\text{Fe}_2\text{Se}]$ Cluster Complexes Relevant to Active Sites of Some Hydrogenases. *Organometallics* **2009**, *28*, 6121–6130. (h) Song, L.-C.; Mei, S.-Z.; Feng, C.-P.; Gong, F.-H.; Ge, J.-H.; Hu, Q.-M. Reactions of Monoanions $[(\mu\text{-RE})(\mu\text{-E})\text{Fe}_2(\text{CO})_6]^-$ and Dianions $[(\mu\text{-E})_2\text{Fe}_2(\text{CO})_6]^{2-}$ (E = Se, S) with N-Substituted Benzimidazolyl Chlorides, Leading to Novel Butterfly Fe/E Cluster Complexes. *Organometallics* **2010**, *29*, 5050–5060.

(18) (a) Apfel, U.-P.; Halpin, Y.; Görls, H.; Vos, G. J.; Weigand, W. Influence of the Introduction of Cyanido and Phosphane Ligands in Multifunctionalized (Mercaptomethyl)silane $[\text{FeFe}]$ Hydrogenase Model Systems. *Eur. J. Inorg. Chem.* **2011**, *2011*, 581–588. (b) Razavet, M.; Davies, S. C.; Hughes, D. L.; Barclay, J. E.; Evans, D. J.; Fairhurst, S. A.; Liu, X.; Pickett, C. J. All-Iron Hydrogenase: Synthesis, Structure and Properties of $\{2\text{Fe}_3\text{S}\}$ -Assemblies Related to the Di-Iron Sub-Site of the H-Cluster. *Dalton Trans.* **2003**, 586–595. (c) Gloaguen, F.; Lawrence, J. D.; Schmidt, M.; Wilson, S. R.; Rauchfuss, T. B. Synthetic and Structural Studies on $[\text{Fe}_2(\text{SR})_2(\text{CN})_x(\text{CO})_{6-x}]^x$ as Active Site Models for Fe-Only Hydrogenases. *J. Am. Chem. Soc.* **2001**, *123*, 12518–12527. (d) Le Cloirec, A.; Best, S. P.; Borg, S.; Davies, S. C.; Evans, D. J.; Hughes, D. L.; Pickett, C. J. A Di-iron Dithiolate Possessing Structural Elements of the Carbonyl/Cyanide Sub-Site of the H-Centre of Fe-Only Hydrogenase. *Chem. Commun.* **1999**, 2285–2286.

(19) (a) Song, L.-C.; Yang, Z.-Y.; Bian, H.-Z.; Liu, Y.; Wang, H.-T.; Liu, X.-F.; Hu, Q.-M. Diiron Oxadithiolate Type Models for the Active Site of Iron-Only Hydrogenases and Biomimetic Hydrogen Evolution Catalyzed by $\text{Fe}_2(\mu\text{-SCH}_2\text{OCH}_2\text{S}\mu)(\text{CO})_6$. *Organometallics* **2005**, *24*, 6126–6135. (b) Song, L.-C.; Li, Q.-L.; Feng, Z.-H.; Sun, X.-J.; Xie, Z.-J.; Song, H.-B. Synthesis, Characterization, and Electrochemical Properties of Diiron Propanedithiolate (PDTe) Complexes as Active Site Models of $[\text{FeFe}]$ -Hydrogenases. *Dalton Trans.* **2013**, *42*, 1612–1626. (c) Thomas, C. M.; Rudiger, O.; Liu, T.; Carson, C. E.; Hall, M. B.; Darensbourg, M. Y. Synthesis of Carboxylic Acid-Modified $[\text{FeFe}]$ -Hydrogenase Model Complexes Amenable to Surface Immobilization. *Organometallics* **2007**, *26*, 3976–3984. (d) Ezzaher, S.; Capon, J.-F.; Gloaguen, F.; Petillon, F. Y.; Schollhammer, P.; Talarmin, J.; Kervarec, N. Influence of a Pendant Amine in the Second Coordination Sphere on Proton Transfer at a Dissymmetrically Disubstituted Diiron System Related to the $[2\text{Fe}]_2\text{H}$ Subsite of $[\text{FeFe}]_2\text{H}_2$ ase. *Inorg. Chem.* **2009**, *48*, 2–4. (e) Li, P.; Wang, M.; He, C.; Liu, X.; Jin, K.; Sun, L. Phosphane and Phosphite Asymmetrically Disubstituted Diiron Complexes Related to the Fe-Only Hydrogenase Active Site. *Eur. J. Inorg. Chem.* **2007**, *2007*, 3718–3727. (f) Morvan, D.; Capon, J.-F.; Gloaguen, F.; Schollhammer, P.; Talarmin, J. Electrochemical Synthesis of Mono- and Disubstituted Diiron Dithiolate Complexes as Models for the Active Site of Iron-Only Hydrogenases. *Eur. J. Inorg. Chem.* **2007**, *2007*, 5062–5068. (g) Gao, Ekstrom, W. J.; Liu, J.; Chen, C.; Eriksson, L.; Weng, L.; Åkermark, B.; Sun, L. Binuclear Iron–Sulfur Complexes with Bidentate Phosphine Ligands as Active Site Models of Fe-Hydrogenase and Their Catalytic Proton Reduction. *Inorg. Chem.* **2007**, *46*, 1981–1991. (h) Song, L.-C.; Li, C.-G.; Ge, J.-H.; Yang, Z.-Y.; Wang, H.-T.; Zhang, J.; Hu, Q.-M. Synthesis and Structural Characterization of the Mono- and Diphosphine-Containing Diiron Propanedithiolate Complexes Related to $[\text{FeFe}]$ -Hydrogenases. Biomimetic H_2 Evolution Catalyzed by $(\mu\text{-PDT})\text{Fe}_2(\text{CO})_4[(\text{Ph}_2\text{P})_2\text{N}(\text{n-Pr})]$. *J. Inorg. Biochem.* **2008**, *102*, 1973–1979. (i) Ezzaher, S.; Capon, J.-F.; Gloaguen, F.; Petillon, F. Y.; Schollhammer, P.; Talarmin, J. Electron-Transfer-Catalyzed Rearrangement of Unsymmetrically Substituted Diiron Dithiolate Complexes Related to the Active Site of the $[\text{FeFe}]$ -Hydrogenases. *Inorg.*

Chem. **2007**, *46*, 9863–9872. (j) Jablonskytė, A.; Wright, J. A.; Pickett, C. J. $[\text{FeFe}]$ -Hydrogenase Models: Unexpected Variation in Protonation Rate between Dithiolate Bridge Analogues. *Eur. J. Inorg. Chem.* **2011**, *2011*, 1033–1037. (k) Liu, Y.-C.; Lee, C.-H.; Lee, G.-H.; Chiang, M.-H. Influence of a Redox-Active Phosphane Ligand on the Oxidations of a Diiron Core Related to the Active Site of Fe-Only Hydrogenase. *Eur. J. Inorg. Chem.* **2011**, *2011*, 1155–1162. (l) Almazahreh, L. R.; Imhof, W.; Talarmin, J.; Schollhammer, P.; Görls, H.; El-khateeb, M.; Weigand, W. Ligand Effects on the Electrochemical Behavior of $[\text{Fe}_2(\text{CO})_5(\text{L})\{\mu-(\text{SCH}_2)_2(\text{Ph})\text{P}=\text{O}\}]$ (L = PPh_3 , $\text{P}(\text{OEt})_3$) Hydrogenase Model Complexes. *Dalton Trans.* **2015**, *44*, 7177–7189.

(20) (a) Tye, J. W.; Lee, J.; Wang, H.-W.; Mejia-Rodriguez, R.; Reibenspies, J. H.; Hall, M. B.; Darensbourg, M. Y. Dual Electron Uptake by Simultaneous Iron and Ligand Reduction in an N-Heterocyclic Carbene Substituted $[\text{FeFe}]$ Hydrogenase Model Compound. *Inorg. Chem.* **2005**, *44*, 5550–5552. (b) Thomas, C. M.; Liu, T.; Hall, M. B.; Darensbourg, M. Y. Series of Mixed Valent Fe(II)Fe(I) Complexes That Model the H_{ox} State of $[\text{FeFe}]$ -Hydrogenase: Redox Properties, Density-Functional Theory Investigation, and Reactivities with Extrinsic CO. *Inorg. Chem.* **2008**, *47*, 7009–7024. (c) Liu, T.; Darensbourg, M. Y. A Mixed-Valent, Fe(II)Fe(I), Diiron Complex Reproduces the Unique Rotated State of the $[\text{FeFe}]$ Hydrogenase Active Site. *J. Am. Chem. Soc.* **2007**, *129*, 7008–7009.

(21) (a) Hsieh, C.-H.; Erdem, Ö.-F.; Harman, S. D.; Singleton, M. L.; Reijerse, E.; Lubitz, W.; Popescu, C. V.; Reibenspies, J. H.; Brothers, S. M.; Hall, M. B.; Darensbourg, M. Y. Structural and Spectroscopic Features of Mixed Valent $\text{Fe}^{\text{II}}\text{Fe}^{\text{I}}$ Complexes and Factors Related to the Rotated Configuration of Diiron Hydrogenase. *J. Am. Chem. Soc.* **2012**, *134*, 13089–13102. (b) Justice, A. K.; Rauchfuss, T. B.; Wilson, S. R. Unsaturated, Mixed-Valence Diiron Dithiolate Model for the H_{ox} State of the $[\text{FeFe}]$ Hydrogenase. *Angew. Chem., Int. Ed.* **2007**, *46*, 6152–6154. (c) Olsen, M. T.; Bruschi, M.; De Gioia, L.; Rauchfuss, T. B.; Wilson, S. R. Nitrosyl Derivatives of Diiron(I) Dithiolates Mimic the Structure and Lewis Acidity of the $[\text{FeFe}]$ -Hydrogenase Active Site. *J. Am. Chem. Soc.* **2008**, *130*, 12021–12030.

(22) (a) Hu, M.-Q.; Ma, C.-B.; Si, Y.-T.; Chen, C.-N.; Liu, Q.-T. Diiron Models for the Active Site of Fe-Only Hydrogenase with Terminal Organosulfur Ligation: Synthesis, Structures and Electrochemistry. *J. Inorg. Biochem.* **2007**, *101*, 1370–1375. (b) Razavet, M.; Davies, S. C.; Hughes, D. L.; Pickett, C. J. $\{2\text{Fe}_3\text{S}\}$ Clusters Related to the Di-Iron Sub-Site of the H-Centre of All-Iron Hydrogenases. *Chem. Commun.* **2001**, 847–848. (c) Lawrence, J. D.; Li, H.; Rauchfuss, T. B. Beyond Fe-Only Hydrogenases: N-Functionalized 2-Aza-1,3-Dithiolates $\text{Fe}_2[(\text{SCH}_2)_2\text{NR}](\text{CO})_x$ (x = 5, 6). *Chem. Commun.* **2001**, 1482–1483. (d) Song, L.-C.; Yang, Z.-Y.; Bian, H.-Z.; Hu, Q.-M. Novel Single and Double Diiron Oxadithiolates as Models for the Active Site of $[\text{Fe}]$ -Only Hydrogenases. *Organometallics* **2004**, *23*, 3082–3084. (e) Daraosheh, A. Q.; Harb, M. K.; Windhager, J.; Görls, H.; El-khateeb, M.; Weigand, W. Substitution Reactions at $[\text{FeFe}]$ Hydrogenase Models Containing $[2\text{Fe}_3\text{S}]$ Assembly by Phosphine or Phosphite Ligands. *Organometallics* **2009**, *28*, 6275–6280.

(23) (a) Song, C.-L.; Fan, H.-T.; Hu, Q.-M. The First Example of Macrocycles Containing Butterfly Transition Metal Cluster Cores via Novel Tandem Reactions. *J. Am. Chem. Soc.* **2002**, *124*, 4566–4567. (b) Song, L.-C.; Gao, J.; Wang, H.-T.; Hua, Y.-J.; Fan, H.-T.; Zhang, X.-G.; Hu, Q.-M. Synthesis and Structural Characterization of Metallocrown Ethers Containing Butterfly Fe_2S_2 Cluster Cores. Biomimetic Hydrogen Evolution Catalyzed by $\text{Fe}_2(\mu\text{-SCH}_2\text{CH}_2\text{OCH}_2\text{CH}_2\text{S}\mu)(\text{CO})_6$. *Organometallics* **2006**, *25*, 5724–5729. (c) Liu, Y.-C.; Tu, L.-K.; Yen, T.-H.; Lee, G.-H.; Yang, S.-T.; Chiang, M.-H. Secondary Coordination Sphere Interactions within the Biomimetic Iron Azadithiolate Complexes Related to Fe-Only Hydrogenase: Dynamic Measure of Electron Density about the Fe Sites. *Inorg. Chem.* **2010**, *49*, 6409–6420. (d) Zhang, Y.; Si, Y.-T.; Hu, M.-Q.; Chen, C.-N.; Liu, Q.-T. Bis(μ^4 -Butane-1,4-dithiolato)bis-[hexacarbonyldiiron(II)(Fe–Fe)]. *Acta Crystallogr., Sect. C: Cryst. Struct. Commun.* **2007**, *63*, m499–m500. (e) Apfel, U.-P.; Halpin, Y.;

- Görls, H.; Vos, J.-G.; Schweizer, B.; Linti, G.; Weigand, W. Synthesis and Characterization of Hydroxy-Functionalized Models for the Active Site in Fe-Only-Hydrogenases. *Chem. Biodiversity* **2007**, *4*, 2138–2148.
- (f) Liu, Y.-C.; Tu, L.-K.; Yen, T.-H.; Lee, G.-H.; Chiang, M.-H. Influences on the Rotated Structure of Diiron Dithiolate Complexes: Electronic Asymmetry vs. Secondary Coordination Sphere Interaction. *Dalton Trans.* **2011**, *40*, 2528–2541.
- (g) Gao, W.; Liu, J.; Åkermarck, B.; Sun, L. Bidentate Phosphine Ligand Based Fe₂S₂-Containing Macromolecules: Synthesis, Characterization, and Catalytic Electrochemical Hydrogen Production. *Inorg. Chem.* **2006**, *45*, 9169–9171.
- (h) Song, L.-C.; Gong, F.-H.; Meng, T.; Ge, J.-H.; Cui, L.-N.; Hu, Q.-M. General Synthetic Route to Double-Butterfly Fe/S Cluster Complexes via Reactions of the Dianions $\{[(\mu\text{-CO})\text{Fe}_2(\text{CO})_6]_2(\mu\text{-SZS}\text{-}\mu)\}^{2-}$ with Electrophiles. *Organometallics* **2004**, *23*, 823–831.
- (i) Abul-Futouh, H.; Görls, H.; Weigand, W. A New Macrocyclic [FeFe]-Hydrogenase H Cluster model. *Phosphorus, Sulfur Silicon Relat. Elem.* **2017**, *192*, 634–637.
- (j) Chiang, M.-H.; Liu, Y.-C.; Yang, S.-T.; Lee, G.-H. Biomimetic Model Featuring the NH Proton and Bridging Hydride Related to a Proposed Intermediate in Enzymatic H₂ Production by Fe-Only Hydrogenase. *Inorg. Chem.* **2009**, *48*, 7604–7612.
- (24) (a) Munery, S.; Capon, J.-F.; De Gioia, L.; Elleouet, C.; Greco, C.; Pétilion, F. Y.; Schollhammer, P.; Talarmin, J.; Zampella, G. New Fe^I–Fe^I Complex Featuring a Rotated Conformation Related to the [2Fe]_H Subsite of [Fe–Fe] Hydrogenase. *Chem. - Eur. J.* **2013**, *19*, 15458–15461. (b) Wang, W.; Rauchfuss, T. B.; Moore, C. E.; Rheingold, A. L.; De Gioia, L.; Zampella, G. Crystallographic Characterization of a Fully Rotated, Basic Diiron Dithiolate: Model for the H_{red} State? *Chem. - Eur. J.* **2013**, *19*, 15476–15479. (c) Goy, R.; Bertini, L.; Elleouet, C.; Görls, H.; Zampella, G.; Talarmin, J.; De Gioia, L.; Schollhammer, P.; Apfel, U.-P.; Weigand, W. A Sterically Stabilized Fe^I–Fe^I Semi-Rotated Conformation of [FeFe] Hydrogenase Subsite Model. *Dalton Trans.* **2015**, *44*, 1690–1699.
- (25) (a) Zhao, J.; Wei, Z.; Zeng, X.; Liu, X. Three Diiron Complexes Bearing an Aromatic Ring as Mimics of the Diiron Subunit of [FeFe]-Hydrogenase: Synthesis, Electron Transfer and Coupled Chemical Reactions. *Dalton Trans.* **2012**, *41*, 11125–11133. (b) Best, S. P.; Borg, S. J.; White, J. M.; Razavet, M.; Pickett, C. J. On the Structure of a Proposed Mixed-Valent Analogue of the Diiron Subsite of [FeFe]-Hydrogenase. *Chem. Commun.* **2007**, 4348–4350. (c) Borg, S. J.; Behrsing, T.; Best, S. P.; Razavet, M.; Liu, X.; Pickett, C. J. Electron Transfer at a Dithiolate-Bridged Diiron Assembly: Electrocatalytic Hydrogen Evolution. *J. Am. Chem. Soc.* **2004**, *126*, 16988–16999. (d) Schwartz, L.; Ekstrom, J.; Lomoth, R.; Ott, S. Dynamic Ligation at the First Amine-Coordinated Iron Hydrogenase Active Site Mimic. *Chem. Commun.* **2006**, 4206–4208. (e) Streich, D.; Karnahl, M.; Astuti, Y.; Cady, C. W.; Hammarstrom, L.; Lomoth, R.; Ott, S. Comparing the Reactivity of Benzenedithiolate- versus Alkyldithiolate-Bridged Fe₂(CO)₆ Complexes with Competing Ligands. *Eur. J. Inorg. Chem.* **2011**, *2011*, 1106–1111. (f) Qian, G.; Wang, H.; Zhong, W.; Liu, X. Electrochemical Investigation into the Electron Transfer Mechanism of a Diiron Hexacarbonyl Complex Bearing a Bridging Naphthalene Moiety. *Electrochim. Acta* **2015**, *163*, 190–195. (g) Gloaguen, F.; Rauchfuss, T. B. Small Molecule Mimics of Hydrogenases: Hydrides and Redox. *Chem. Soc. Rev.* **2009**, *38*, 100–108.
- (26) (a) Ortega-Alfaro, M. C.; Hernández, N.; Cerna, I.; López-Cortés, J. G.; Gómez, E.; Toscano, R. A.; Alvarez-Toledano, C. Novel Dinuclear Iron(0) Complexes from α,β -Unsaturated Ketones β -Positioned with Sulfide and Sulfoxide Groups. *J. Organomet. Chem.* **2004**, *689*, 885–893. (b) Lyon, E. J.; Georgakaki, I. P.; Reibenspies, J. H.; Darensbourg, M. Y. Carbon Monoxide and Cyanide Ligands in a Classical Organometallic Complex Model for Fe-Only Hydrogenase. *Angew. Chem., Int. Ed.* **1999**, *38*, 3178–3180.
- (27) Goodrow, M. H.; Musker, W. K. Synthesis of Medium Ring Disulfides by Titrimetry; An Improvement on High Dilution Techniques. *Synthesis* **1981**, *1981*, 457–459.
- (28) (a) Noureldin, N. A.; Caldwell, M.; Hendry, J.; Lee, D. G. Heterogeneous Permanganate Oxidation of Thiols. *Synthesis* **1998**, 1587–1589. (b) Kato, E.; Oya, M.; Iso, T.; Iwao, J.-I. Conversion of Thiols into Disulfides with Diethyl Bromomalonate. *Chem. Pharm. Bull.* **1986**, *34*, 486–495. (c) Harpp, D. N.; Bodzay, S. J.; Aida, T.; Chan, T. H. High Yield Preparation of Cyclic Disulfides Using Alkyltin Thiolates. *Tetrahedron Lett.* **1986**, *27*, 441–444. (d) Affleck, J. G.; Dougherty, G. The Preparation and Relative Reactivities of Many-Membered Cyclic Disulfides. *J. Org. Chem.* **1950**, *15*, 865–868. (e) Ma, M.; Zhang, X.; Peng, L.; Wang, J. Electrophilic Reaction of Nitric Oxide with Wittig Reagents. *Tetrahedron Lett.* **2007**, *48*, 1095–1097.
- (29) (a) Groth, P. The Crystal Conformations of Cyclotetraeicosane and Cyclohexaeicosane at –160 °C. *Acta Chem. Scand.* **1979**, *33a*, 199–201. (b) Newman, B. A.; Kay, H. F. Chain Folding in Polyethylene and Cyclic Paraffins. *J. Appl. Phys.* **1967**, *38*, 4105–4109. (c) Holleman, A. F.; Wiberg, N. *Lehrbuch der Anorganischen Chemie*; Walter de Gruyter Verlag: Berlin, 1995.
- (30) Nametkin, N. S.; Tyurin, V. D.; Kukina, M. A. Synthesis and Some Properties of Sulfur-Containing Iron Tricarbonyl Complexes. *J. Organomet. Chem.* **1978**, *149*, 355–370.
- (31) Compound **13** was previously reported by Seyferth et al. using the synthetic pathway shown in Scheme 1A. See: Seyferth, D.; Henderson, R. S.; Song, L.-C. The Dithiobis(tricarbonyliron) Dianion: Improved Preparation and New Chemistry. *J. Organomet. Chem.* **1980**, *192*, C1–C5. Indeed, several attempts were carried out to obtain complex **13** by following their method, but unfortunately, without success.
- (32) (a) Felton, G. A. N.; Petro, B. J.; Glass, R. S.; Lichtenberger, D. L.; Evans, D. H. One- to Two-Electron Reduction of an [FeFe]-Hydrogenase Active Site Mimic: The Critical Role of Fluxionality of the [2Fe₂S] Core. *J. Am. Chem. Soc.* **2009**, *131*, 11290–11291. (b) Harb, M. K.; Daraosheh, A.; Görls, H.; Smith, E. R.; Meyer, G. J.; Swenson, M. T.; Sakamoto, T.; Glass, R. S.; Lichtenberger, D. L.; Evans, D. H.; El-khateeb, M.; Weigand, W. Effects of Alkane Linker Length and Chalcogen Character in [FeFe]-Hydrogenase Inspired Compounds. *Heteroat. Chem.* **2014**, *25*, 592–606.
- (33) (a) Lyon, E. J.; Georgakaki, I. P.; Reibenspies, J. H.; Darensbourg, M. Y. *J. Am. Chem. Soc.* **2001**, *123*, 3268–3278. (b) Robin, F.; Rumin, R.; Talarmin, J.; Pétilion, F. Y.; Muir, K. W. *Organometallics* **1993**, *12*, 365–380.
- (34) Crouthers, D. J.; Denny, J. A.; Bethel, R. D.; Munoz, D. G.; Darensbourg, M. Y. Conformational Mobility and Pendent Base Effects on Electrochemistry of Synthetic Analogues of the [FeFe]-Hydrogenase Active Site. *Organometallics* **2014**, *33*, 4747–4755.
- (35) COLLECT Data Collection Software; Nonius B.V.: Delft, The Netherlands, 1998.
- (36) Otwinowski, Z.; Minor, W. Processing of X-Ray Diffraction Data Collected in Oscillation Mode. *Methods Enzymol.* **1997**, *276*, 307–326.
- (37) SADABS, version 2.10; Bruker AXS: Madison, WI, 2002.
- (38) Sheldrick, G. M. A Short History of SHELX. *Acta Crystallogr., Sect. A: Found. Crystallogr.* **2008**, *64*, 112–122.
- (39) Spek, A. L. PLATON SQUEEZE: A Tool for the Calculation of the Disordered Solvent Contribution to the Calculated Structure Factors. *Acta Crystallogr., Sect. C: Struct. Chem.* **2015**, *71*, 9–18.